UNIVERSITÀ
DI PAVIA

DIPARTIMENTO DI SCIENZE DEL FARMACO

Direttrice Chiar.ma Prof.ssa Simona Collina

LAUREA MAGISTRALE A CICLO UNICO IN CHIMICA E TECNOLOGIA FARMACEUTICHE

Development of Global ubiquitinome analysis to study LRRK2 mediated signalling in mouse embryonic fibroblasts of wild-type and D620N VPS35

Sviluppo di una metodologia di analisi dell'ubiquitinoma per lo studio della trasduzione del segnale mediata da LRRK2 in fibroblasti embrionali murini wild-type e VPS35 D620N

Relatore: *Prof.ssa Sofia Giorgetti*

Correlatore: *Prof. Dario Renato Alessi*

Gaia D'Anna
Matricola: *488754*

Anno Accademico 2024/2025

INDEX

1. Abstract

Parkinson's disease (PD) is a progressive neurodegenerative movement disorder characterized by the loss of dopaminergic neurons and the accumulation of misfolded proteins. The VPS35 [D620N] mutation, associated with familial PD, was found to enhance Leucine-rich Repeat Kinase-2 (LRRK2) activity and disrupt lysosomal protein levels through proteasomal degradation. However, the molecular mechanisms linking LRRK2 hyperactivation to the ubiquitin-proteasome system (UPS) are still not fully understood.

This work focused on developing and optimizing a methodology for the comprehensive analysis of the ubiquitinome in wild-type and VPS35 [D620N] mouse embryonic fibroblasts (MEFs), to investigate LRRK2-mediated signalling.

Three distinct protocols, based on different extraction methods (urea, SDS and sodium deoxycholate) were tested, and the resulting ubiquitinome data were compared.
The optimized SDS-based workflow was chosen as the most suitable one as it proved to be reproducible and sensitive, while still being straightforward.

Ubiquitinome profiling revealed that VPS35 [D620N] MEFs display increased ubiquitylation of LRRK2-dependent endolysosomal proteins, including several Rab GTPases (LRRK2 substrates). This is consistent with the enhanced LRRK2 kinase activity observed in the mutant. Moreover, pharmacological inhibition of LRRK2 with MLi-2 markedly reduced the ubiquitylation of these substrates, as well as Hedgehog-, Parkinson's disease- and UPS-associated proteins when compared to their levels in the WT. Quantitative proteomics showed increased steady-state protein levels upon LRRK2 inhibition in the VPS35 [D620N] background.

Collectively, these findings suggest that hyperactivation of LRRK2 in VPS35 [D620N] cells may lead to the degradation of specific signalling components via ubiquitylation, whereas inhibition of LRRK2 restores their whole-cell levels.

Overall, this study established a robust analytical methodology for ubiquitinome profiling and provides new insights into the molecular interplay between LRRK2 and the UPS in Parkinson's disease pathogenesis.

Il morbo di Parkinson è una patologia neurodegenerativa progressiva, associata a sintomatologia motoria e non motoria, caratterizzata dalla perdita dei neuroni dopaminergici e dall'accumulo di proteine misfolded. Da studi pregressi è emerso che la mutazione [D620N] di VPS35, associata a forme ereditarie di Parkinson, causa un aumento dell'attività chinasica di LRRK2 (Leucine-rich Repeat Kinase-2) e altera i livelli delle proteine lisosomiali attraverso la degradazione proteosomica. Tuttavia, i meccanismi molecolari che legano l'iperattivazione di LRRK2 al sistema ubiquitina-proteosoma (UPS) non sono ancora del tutto chiari.

Questo lavoro di ricerca si è concentrato sullo sviluppo e l'ottimizzazione di una metodologia per l'analisi completa dell'ubiquitinoma in fibroblasti embrionali murini (MEF) wild-type e VPS35 [D620N], al fine di studiare la segnalazione mediata da LRRK2.

Sono stati testati tre protocolli distinti, basati su diversi metodi di estrazione (urea, SDS e desossicolato di sodio), e sono stati confrontati i dati dell'ubiquitinoma ottenuti. Tra le tre metodologie, quella basata su SDS è stata ritenuta la più adatta allo scopo previsto, in quanto il metodo si è dimostrato riproducibile, sensibile e di facile applicazione.

Il profilo dell'ubiquitinoma ha rivelato che i MEF VPS35 [D620N] mostrano un aumento dell'ubiquitinazione delle proteine endolisosomiali dipendenti da LRRK2, tra cui diverse Rab GTPasi (substrati di LRRK2). Ciò è coerente con l'aumentata attività enzimatica di LRRK2 osservata nel mutante. Inoltre, l'inibizione farmacologica di LRRK2 con MLi-2 ha ridotto notevolmente l'ubiquitinazione di questi substrati, così come delle proteine associate a Hedgehog, al morbo di Parkinson e all'UPS in confronto ai loro livelli nel WT. Dall'analisi proteomica quantitativa è emerso un aumento dei livelli proteici allo stato stazionario in seguito all'inibizione di LRRK2 nel contesto VPS35 [D620N].

Nel complesso, questi risultati suggeriscono che l'iperattivazione di LRRK2 nelle cellule VPS35 [D620N] può portare alla degradazione di specifici componenti di segnalazione tramite ubiquitinazione, mentre l'inibizione di LRRK2 ripristina i loro livelli cellulari.

In conclusione, questo studio ha stabilito una metodologia analitica robusta per la caratterizzazione dell'ubiquitinoma e ha permesso di ottenere informazioni preliminari sull'interazione molecolare tra LRRK2 e il sistema ubiquitina-proteosoma nella patogenesi del morbo di Parkinson.

2. Introduction

2.1. Parkinson's Disease and associated pathological mutations

Epidemiology, Clinical features and Diagnostic criteria

Parkinson's disease (PD) is a progressive neurodegenerative movement disorder with a high prevalence in middle-aged and elderly people. Its global burden has significantly increased over the past few decades. A recent study on the evolution of Parkinson's disease from 1990 to 2021 showed that in 2021, 11.77 million people worldwide were affected by the disease, and 0,13 million new cases were reported, which increased by 273.76% and 220.07%, respectively, compared to 1990. [1] PD is characterized by motor symptoms, including bradykinesia, muscle stiffness, resting tremor, and postural instability, and non-motor features, including pain, fatigue, autonomic dysfunction, and sleep behaviour disorders. [2] Parkinson's disease (PD) progresses in a selective pattern in brain regions, largely driven by the spread of misfolded α-synuclein. The classical Braak model proposes a caudorostral sequence, starting in the olfactory bulb and lower brainstem, then advancing to the midbrain (including the substantia nigra) and limbic areas, and finally the cortex, explaining early non-motor symptoms before motor onset. [3] The International Parkinson and Movement Disorder Society (MDS) has developed criteria to improve diagnostic accuracy. These guidelines define Parkinson's syndrome as the presence of bradykinesia plus at least one additional cardinal motor sign (rest tremor or limb rigidity). The MDS criteria emphasize progression, asymmetry, and response to dopaminergic therapy, while clearly listing red-flag features that argue against PD. [4]

Molecular mechanisms

Parkinson's disease (PD) is driven by different molecular pathways that promote the loss of dopaminergic neurons. The hallmark event is the misfolding and aggregation of α-synuclein into oligomers and Lewy body fibrils, which disrupts synaptic vesicle trafficking, impairs proteasomal and autophagic clearance, and directly damages mitochondria. Another cause of neuronal degeneration is oxidative stress, which is caused by excessive reactive oxygen species (ROS) generated by NADPH oxidase (NOX) and dysfunctional mitochondria. Moreover, ferroptosis, an iron-dependent form of regulated cell death, is triggered by disrupted iron homeostasis, lipid peroxidase accumulation, and glutathione peroxidase 4 (GPX4) depletion. Iron overload in microglia and neurons accelerates ROS production and neuronal demise. In addition, mitochondrial dysfunction, caused by complex I inhibition or genetic mutations, leads to impaired oxidative phosphorylation, reduced ATP and increased ROS levels, which together promote neurodegeneration. Chronic neuroinflammation is enhanced by activated microglia and astrocytes that release cytokines via the NFκB and NLRP3 inflammasome pathways. α-Synuclein acts as a damage-associated molecular pattern that stimulates innate immune receptors. Moreover, gut dysbiosis contributes to PD by increasing intestinal permeability and exposing the enteric nervous system to bacterial products that promote α-synuclein aggregation and propagate pathology. These mechanisms interact dynamically, creating a self-reinforcing cycle that underlies the progressive loss of substantia nigra dopaminergic neurons in PD. [5], [6], [7]

Etiology and Pathogenesis

Most PD cases are idiopathic, and only approximately 10–15% are linked to known genetic mutations. Environmental risk factors, such as stress, brain damage, physical inactivity, and pesticide exposure, also play an important role in the onset of the disease. Only 5–10% of patients with PD suffer from a monogenic form with Mendelian inheritance, which means that it is caused by a mutated single gene and can be passed down in families through autosomal dominant or autosomal recessive patterns. In the former, one copy of a gene

variant is needed to cause the genetic condition, while autosomal recessive means two copies of the gene variant are required for the condition to manifest. Autosomal dominant (AD) Parkinson's disease is caused by mutations in a small set of genes: SNCA (encoding α-synuclein), leucine-rich repeat kinase 2 (LRRK2), vacuolar protein sorting 35 (VPS35), and eukaryotic-translation-initiation-factor 4-γ-1 (EIF4G1). Mutations in SNCA are rare and result in an increasing formation of α-synuclein oligomers and fibrils that disrupt synaptic membranes and vesicle cycling. EIF4G1 missense mutations (p.R1205H, p.A502V) disrupt the eIF4F translation initiation complex, reducing the synthesis of mitochondrial, cell survival and growth proteins, promoting neurotoxicity. LRRK2 and VPS35 mutations will be discussed later in further detail.

In contrast, autosomal recessive Parkinson's disease (AR-PD) is caused by mutations in several genes implicated in mitochondrial and protein degradation pathways. One of these genes is PARK2 (PRKN) that encodes for the E3 ubiquitin-ligase parkin. Generally, Parkin is localized in the cytosol except in case of mitochondrial damage when it gets phosphorylated by PINK1 (PTEN-induced putative kinase 1) and transported to the mitochondria to ubiquitilate mitochondrial membrane proteins. These modifications act as a signal of mitophagy. Mutations of both PARK2 or PINK1 genes result in the accumulation of dysfunctional mitochondria leading to early-onset PD. Another gene involved in the pathogenesis of PD is PARK7, encoding for the peptidase DJ-1, which functions as a redox-sensitive chaperone and antioxidant. Mutations of PARK7 increase neuronal vulnerability to oxidative damage and lead to stress-induced apoptosis. Other rare forms of recessive inherited PD are caused by mutations in ATP13A2, PLA2G6 and FBXO genes. The first one is a lysosomal P5-type ATPase involved in endosome-lysosome transport and protects cells from Mn^{2+} and Zn^{2+} induced toxicity. Loss of function mutations disrupt lysosomal homeostasis, leading to α-synuclein accumulation and neurodegeneration. PLA2G6 gene encodes for a phospholipase A2 involved in lipid metabolism, hence in cell membrane homeostasis. Recessive mutations result in lipid peroxidation, promoting

mitochondrial membrane instability and neuronal loss. The latter, FBXO7 directly interacts with Parkin and PINK1 during stress-induced mitophagy. Mutations in FBXO7 leads to its mislocalization to the cytosol, compromising mitophagy. [8], [9]

2.2. LRRK2 and associated pathological mutations

Structure and Mechanism of LRRK2

Leucine-rich repeat kinase 2 (LRRK2) is a 288-kDa polypeptide that includes seven sequential domains: armadillo repeats (ARM), ankyrin repeats (ANK), leucine-rich repeats (LRR), an unusual Roco family GTPase consisting of a GTP-binding ROC domain connected to two COR domains (COR-A and COR-B), a kinase (KIN), and WD40 domains. The LRR domain contains a short hinge helix that links ARM to WD40, while a C-terminal helix contacts ANK, COR, and KIN, stabilizing the overall J-shaped monomer (**Figure 2.2*a***). LRRK2 is a ubiquitously expressed protein, but its highest cellular levels are found in immune cells, particularly in macrophages, monocytes, and neutrophils. Apart from the immune system, LRRK2 is highly found in lungs, kidney and pancreas, and least expressed in the brain. It is implicated in vesicular trafficking, autophagy, lysosome function and ciliogenesis. [10]

LRRK2 phosphorylates a subset of small Rab-GTPases (Rab3A/B/C/D, Rab8A/B, Rab10, Rab12, Rab29, Rab35, and Rab43) involved in vesicle formation, vesicle docking and fusion, and cytoskeletal motility. Rabs interconvert between their active GTP-bound form and inactive GDP-bound state through dedicated guanine nucleotide exchange factors (GEFs) and GTPase-activating proteins (GAPs). After vesicle transfer, Rabs are retrieved from the target membranes and redelivered to their membrane of origin by cytosolic GDP-binding proteins called GDIs (**Figure 2.1**). The domains of Rab proteins that change conformation between the active and inactive states are the so-called Switch I and Switch II regions. LRRK2 phosphorylates its Rabs

within their Switch II domain, blocking their ability to bind to GDIs or effector proteins, thereby blocking their GTPase function. [11], [12], [13]

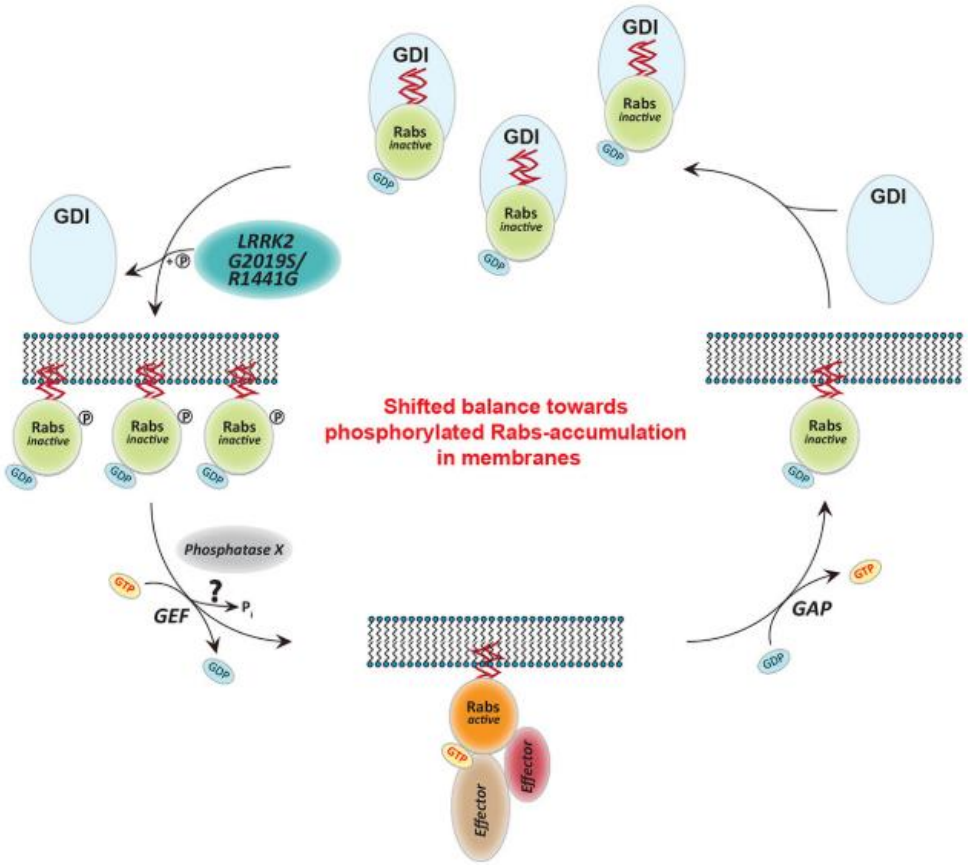

Figure 2.22.1 Model of Rab GTPase phosphorylation by LRRK2 and its outcome. Rab GTPases (Rabs) cycle between an inactive (GDP-bound) and an active state (GTP-bound) between cytosol and membranes, respectively. Geranyl-geranyl-modified Rab GTPases in their GDP-bound state are tightly bound by guanine dissociation inhibitors (GDIs) in the cytosol. LRRK2 aids the insertion of Rabs in their specific target membrane. After removal of the LRRK2 phosphorylation site, guanine exchange factors (GEFs) facilitate exchange of GDP to GTP. This in turn allows binding to effector proteins and membrane trafficking events. Next, a Rab-specific GTPase-activating protein (GAP) assists in the hydrolysis of GTP followed by removal of the Rab GTPase from the target membrane by GDIs. In pathogenic conditions, in which LRRK2 is hyperactive, Rab GTPases have strongly diminished affinities for GDIs. As a result, the equilibrium between membrane-bound and cytosolic Rabs is disturbed, which may contribute to LRRK2 mutant carrier disease phenotypes. (Hutagalung et al., 2011)

LRRK2 can be phosphorylated by CK1α at its Ser910 and Ser935, along with nearby Ser955 and Ser973, which are considered biomarker sites because their phosphorylation reflects the conformation of the LRRK2 kinase domain *in vivo*. These sites are typically phosphorylated when the kinase domain is inactive (open conformation). Another key site, Ser1292, located near the C-terminal end of the LRR domain, is a well-known autophosphorylation site. Its phosphorylation directly indicates LRRK2 activity. Some disease-linked mutations, particularly G2019S, increase LRRK2 autophosphorylation at Ser1292. [14] When in its inactive conformation, the N-terminal half of LRRK2 wraps around its enzymatic half, with the LRR domain sterically blocking the binding site of KIN and the ARM domain extends outward. The LRR domain also blocks the C-terminal half by anchoring itself to the WD40 domain via its helix-hinge domain. (**Figure 2.2*a***) [15]

The KIN domain consists of two lobes: the N lobe, composed of a β-sheet-rich amino terminal that binds to ATP and contains a conserved helix, and the C lobe, which consists of a carboxy-terminal portion that binds to the substrates. The C lobe also harbors three critical residues for catalysis: Lys and Glu that position the phosphate of the ATP in the correct conformation to be transferred to the substrate, while an Asp helps coordinate the metal ion. When Mg^{2+}-ATP is bound, the two lobes come closer together to form the active (closed) conformation in which the kinase domain binds and phosphorylates the substrates. (**Figure 2.2*b,c***) [16]

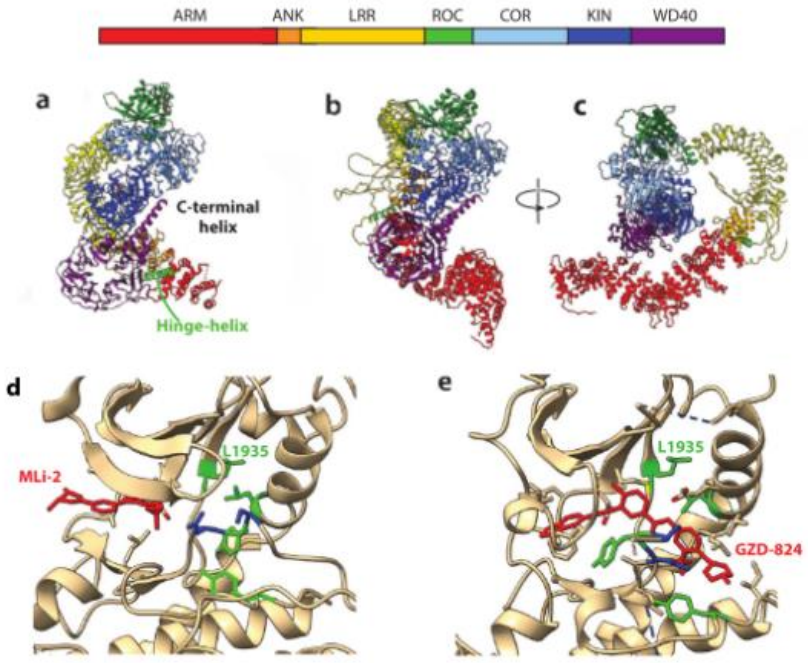

Figure 2.2 LRRK2 structures. The various domains are coloured as shown in the bar above panels a-c: ARM red, ANK orange, LRR yellow, ROC green, COR light blue, KIN dark blue and WD40 in purple. (a) Full-length inactive LRRK2 (PDB ID:7LI4), highlighting the hinge helix and C-terminal helices. (b,c) Two views of the AlphaFold model of LRRK2 (PDB ID: Q5SS007). Structures of LRRK2 G2029S ROC-COR-KIN-WD40 bound to (d) MLi-2 or € GZD-824 (PDB ID: 8TYQ) with ligands shown in red. The DYS motif is shown in blue; the regulatory-spine residues L1935, L1924, Y2018, and Y1992 are shown in green. Note that the residues of the spine are aligned, consistent with a closed, active conformation with the Type I inhibitor MLi-2 bound (panel d); this contrasts with the broken alignment of the regulatory spine residues when the Type II inhibitor GZD-824 is bound (panel e). Abbreviations: ANK, ankyrin repeat; ARM, Armadillo repeat; COR, C-terminal of ROC domain; KIN, kinase domain; LRR, leucine-rich repeat; LRRK2, LRR kinase 2; PDB ID, Protein Data Bank identifier; RCKW, ROC–COR–KIN–WD40; ROC, Ras of complex proteins domain; WD40, WD40 domain. (Alessi and Pfeffer, 2025)

Genetic variants of LRRK2 in Parkinson's Disease

Mutations in LRRK2 account for 1-2% of idiopathic and 5 % of inherited PD cases, making it the most common cause of familial AD PD. Dysfunctional LRRK2 interferes with several cellular pathways, including vesicular transport, cytoskeletal dynamics, mitochondrial trafficking, and lysosomal function, thereby contributing to neuronal dysfunction.[9], [17]

In 2024, Krüger et al. curated a MDS Gene literature review summarizing published demographic, clinical, and genetic findings related to potentially pathogenic LRRK2 variants. Data collected from 3,296 patients with PD allowed the identification of 205 distinct LRRK2 variants: 14 (6.8 %) were classified as pathogenic, 8 (3.9 %) as likely pathogenic, and the remaining 183 (89.3 %) as variants of uncertain significance. The most frequent pathogenic mutation is the pG2019S substitution, which accounts for 73.6 % of all LRRK2-PD cases, followed by p.R1441G and p.R1441C, together representing more than 80 % of carriers. Data have shown that LRRK2 mutations cause late-onset PD with a median age at onset of 56 years.[18]

All established pathogenic mutations implicated in PD enhance LRRK2-mediated Rab phosphorylation. Kalogeropuloua et al. reported 50 variants that activate LRRK2 with many of which located in noncatalytic domains (**figure 2.3**). A mutation is defined as activating when LRRK2 activity is increased by more than 1.5-fold. [19]

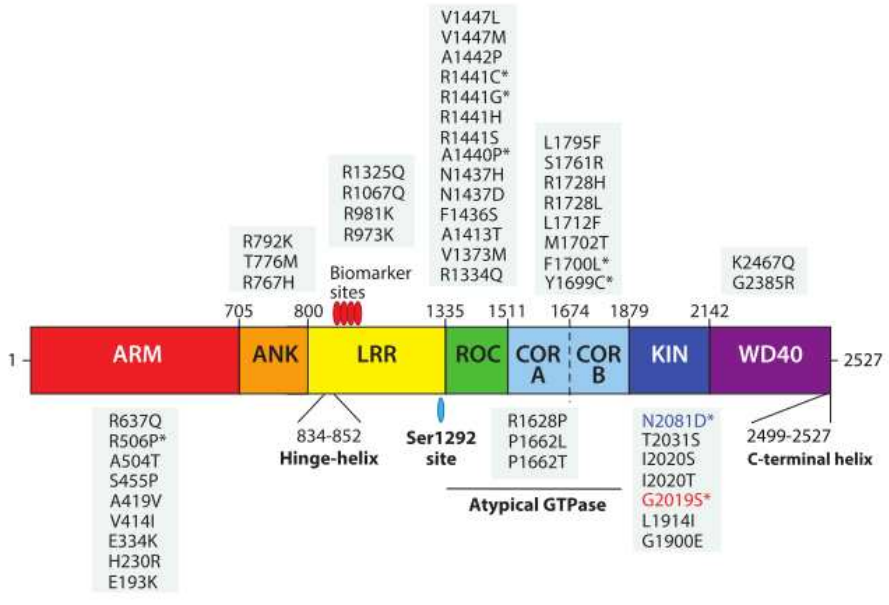

Figure 2.3 Location of 50 LRRK2 variants reported to promote LRRK2 activity at least 1.5-fold, as assessed in a cellular overexpression assay of Rab phosphorylation. Abbreviations: ARM, Armadillo repeat; ANK, ankyrin repeat; LRR, leucine-rich repeat; ROC, Ras of complex proteins domain; COR, C-terminal of ROC domain; KIN, kinase domain; WD40, WD40 domain. (Alessi and Pfeffer, 2025).

Pathogenic mutations cluster at the ROC-COR interface and within the kinase domain, destabilising the inactive (open) conformation, thereby increasing its catalytic activity. This suggests that LRRK2 kinase inhibitors may be useful for treating patients with both idiopathic and familial PDs.

There are two types of kinase inhibitors. Type I compounds bind to the ATP-binding pocket of LRRK2, stabilizing the active-like closed conformation of the enzyme (**figure 2.2*d***). This results in a significant reduction in the phosphorylation of LRRK2 at its biomarker sites (Ser910 and Ser935), which mediate the binding of 14-3-3 proteins. [20] Studies have demonstrated that the loss of 14-3-3 binding promotes LRRK2 aggregation and destabilization in cells. [21] Examples of type I inhibitors are MLi-2 and two compounds currently undergoing clinical trials, DNL151 and DNL201. [22]

In contrast, type II inhibitors, such as GZD-824, block the enzyme in an inactive conformation by occupying an additional binding site immediately near the ATP pocket, which is made accessible by an activation-loop rearrangement characteristic of kinases in the inactive conformation. Type II inhibitors prevent ATP from binding to LRRK2, as these compounds overlap with the ATP-binding site (**figure 2.2*e***). Type II LRRK2 inhibitors block Rab protein phosphorylation without inducing biomarker dephosphorylation. [23] While highly selective Type II LRRK2 inhibitors are currently unavailable, their development could offer significant therapeutic benefits over Type I compounds for treating Parkinson's disease linked to LRRK2.

2.3. Lysosomal dysfunction caused by VPS35 [D620N] mutation

As mentioned earlier, missense mutations in the VPS35 gene result in autosomal dominant PD. Overall, VPS35 mutations are a rare cause of PD accounting for only about 1% of familial parkinsonism and 0.2% of sporadic PD. [9] VPS35 is a key component of the heteropentameric retromer, a protein complex situated in the endosome. This complex is involved in the transport

and recycling of transmembrane protein cargo from the endosome to the Golgi complex and from the endosome to the plasma membrane. [24] To date, only the VPS35 [D620N] mutation, in which the aspartic acid at residue 620 is substituted with an asparagine, has been confirmed as pathogenic, although additional rare PD-causing VPS35 variants have been identified, but not been confirmed. [25] A study conducted on mouse embryonic fibroblasts (MEFs) showed that when knocking-in VPS35 [D620N], phosphorylation of Rab8A, Rab10 (Thr73) and Rab12 significantly increased to 4-6 fold. Moreover, data showed that LRRK2 autophosphorylation at Ser1292 was also heightened, meaning an overall increased kinase activation. [26]

When Rabs are phosphorylated and become immobilized on membranes, they lose their ability to bind to GDIs and, instead, engage with phospho-Rab-specific effectors like RILPL1/2 and JIP3/4. This interaction interferes with vesicular transport, autophagy, lysosomal function and ciliogenesis. The bond occurs between the arginine residue in the RH2 motif, an alpha-helix structure common in RILPL1/2 and JIP3/4, and the phosphorylated residues within the Switch II motif of Rabs. [27] The interaction between pRab10 and RILPL1 affects the formation of primary cilia in both the somatosensory cortex and the dorsal striatum. The absence of primary cilia in the striatum disrupts Hedgehog signalling, which plays a crucial role in supplying neuroprotective factors to DOPA neurons. [28] Additionally, the increase in Rab phosphorylation driven by LRRK2 hinders the axonal transport of autophagosomes and disrupts proper centriolar cohesion. [29]

In 2023, a study conducted on MEFs by Pal et al. demonstrated that lysosomal stress or dysfunction caused by the VPS35 [D620N] mutation or the lysosomotropic agent LLOMe leads to the recruitment of LRRK2 to the lysosome, resulting in phosphorylation of Rab proteins, which triggers recruitment of RILPL1 to the lysosome. This subsequently interacts through its conserved C-terminal region with a conserved domain of TMEM55B, an integral lysosomal membrane protein (**figure 2.4**). TMEM55B is composed of 284 residues and 2 transmembrane domains with N- and C-termini facing the cytosol.

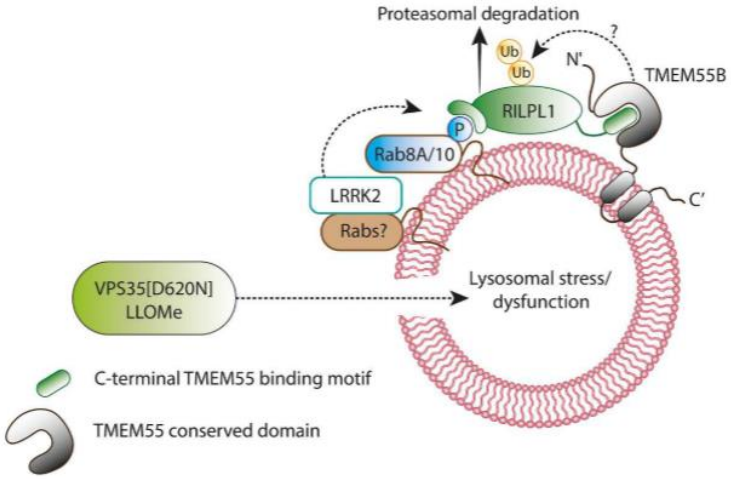

Figure 2.4 Model of how lysosomal dysfunction resulting from VPS35[D620N] mutation recruits and activates LRRK2 to the lysosome, resulting in phosphorylation of Rab proteins, which in turn triggers the recruitment of RILPL1 and its binding to TMEM55B. (Pal et al., 2023)

Recruitment of RILPL1 to the lysosome accelerates its degradation. This has been deducted from mass spectrometry data of whole cell lysate, revealing reduced levels of RILPL1 in the VPS35 [D620N] background (**figure 2.5*a,b***). This loss is reversible by inhibiting LRRK2 kinase activity with MLi-2, indicating that LRRK2 drives the degradation process. MLi-2 brings RILPL1 levels at the VPS35 [D620N] lysosome back to the WT levels within 8 hours. (**figure 2.5*c***). As expected, pRab10 levels dropped when treating with MLi-2 due to LRRK2 inhibition.

To assess whether in VPS35 [D620N] MEFs the degradation of RILPL1 is mediated via lysosomal or proteasomal pathways, the cells were treated with either cycloheximide (a translation inhibitor) alone, or in combination with MG-132 (a proteasome inhibitor), or either a combination of cycloheximide and lysosomal protease inhibitor cocktail for 8 and 12 hours before lysis. Co-treatment with the proteasome inhibitor MG-132 partially restores RILPL1 levels after 8 hours and substantially after 12 hours, whereas lysosomal protease inhibitors have no effect, demonstrating that the degradation is proteasome-mediated (**figure 2.5*d***). [30]

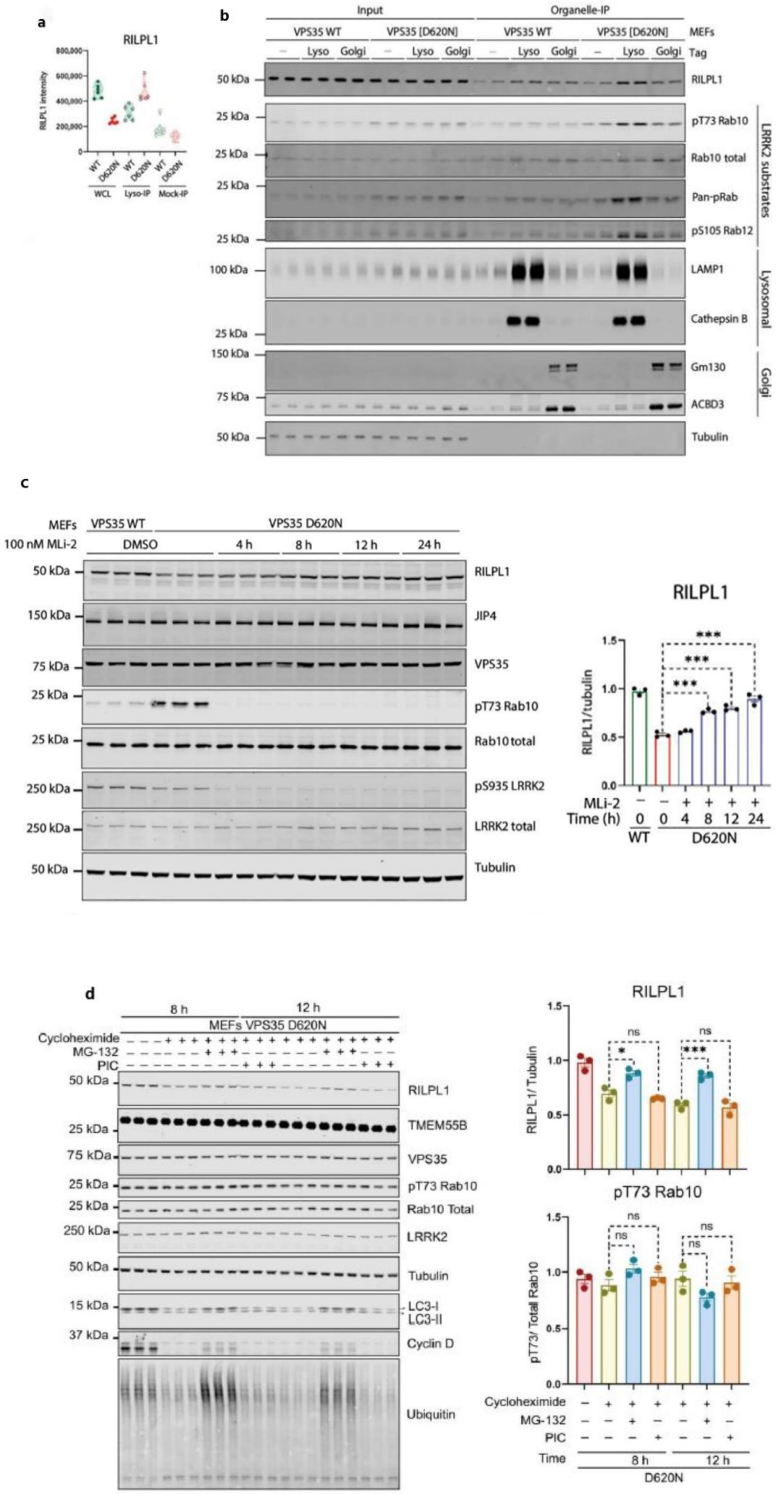

Figure 2.5 Enhanced LRRK2 activity by VPS35[D620N] mutation reduces expression of RILPL1. (a) Violin plot of RILPL1 levels derived from indicated littermate-matched MEFs, transduced ± LysoTag (TMEM192-3xHA) and subjected to LysoTag IP. A sample of the homogenate was removed and designated as WCL. Experiments were performed in six

*technical replicates and analyzed by DIA-MS. (b) Indicated MEFs transduced ± either the LysoTag (TMEM192-3xHA) or GolgiTag (TMEM115-3xHA) were subjected to organelle isolation. Two micrograms of both the immunoprecipitate and respective input (WCL) was subjected to immunoblot analysis using the LI-COR Odyssey CLx Western blot imaging and the indicated antibodies. Each lane indicates a sample derived from a different dish of cells. (c) Littermate-matched WT and VPS35[D620N] homozygous knock-in MEFs were treated ± 100 nM MLi-2 for the indicated times before lysis. Lysates were subjected to quantitative immunoblot analysis of the LI-COR Odyssey CLx Western blot imaging system and indicated antibodies. Technical replicates represent cell extract obtained from a different dish of cells. Quantitation of immunoblotting data is shown as mean ± SEM. Data were analyzed using two-tailed unpaired t test (**P < 0.01,***P < 0.001, and ****P < 0.001). (d) VPS35 [D620N] MEFs were treated with either 50 µg/mL of cycloheximide alone, or cycloheximide+10 µM MG132, or cycloheximide + protease inhibitor cocktails (PIC - 5 µM of E64D + 10 µM of Leupeptin + 10 µM of pepstatin A) for 8 h and 12 h prior to lysis. Lysates were subjected to quantitative immunoblot as described in c. (Modified from Pal et al.,2023)*

2.4. The Ubiquitin-Proteasome System

Besides lysosomes, the primary proteolytic mechanism in eukaryotes is the ubiquitin-mediated proteasomal degradation. Ubiquitylation, a posttranslational modification, is involved in many cellular processes, such as autophagy, DNA repair, cell cycle and, most importantly, protein homeostasis.

Ubiquitin covalently binds to the ε-amino group of a lysine residue of the protein destined to be degraded. It is a small 76 amino acid protein containing seven lysine residues (K-6, 11, 27, 29, 33, 48, and 63) and a N-terminal methionine (M1), all of which provide attachment points for further ubiquitin units during a polyubiquitylation cycle. This leads to the formation of either homotypic chains, where ubiquitin units are linked by a single type of connection, or heterotypic chains, which involve various types of linkages. K48- or K11-linked polyubiquitin chains act as a signal to target proteins for proteasomal degradation. [31]

Ubiquitin is activated through an ATP-dependent process by the ubiquitin-activating enzyme E1, which creates a high-energy thiol bond. The activated ubiquitin is then passed to a ubiquitin-conjugating enzyme E2, preparing it for

conjugation via its C-terminus to a substrate protein. Meanwhile, the substrate protein is recognized by the E3 ubiquitin ligase, which also associates with E2, allowing ubiquitin to first be transferred to the E3 enzyme and then to the substrate (**figure 2.6**). [32] Multiple cycles of this enzymatic cascade occur when ubiquitin is coupled to lysine 48 to form a polyubiquitin chain. Polyubiquitylated proteins are recognized by the proteasome and thereafter degraded. Proteasomes are ubiquitously present in the nucleus and the cytoplasm of all eukaryotic cells. Also known as the 26S proteasome, it is a large (2.5 MDa), dynamic holoenzyme that consists of at least 32 distinct subunits in two copies. The proteasome can be divided into two functional subcomplexes, the 20S proteasome, which carries out the catalytic activity, and the 19S proteasome, which regulates the 20S subunit and prepares the substrates for degradation. [33] The ubiquitin moieties are not degraded when a substrate protein is degraded by the proteasome. Instead, a group of deubiquitylation enzymes (DUBs) cleave off ubiquitin at the amide bond following the last amino acid in ubiquitin, acting as cysteine proteases. [34]

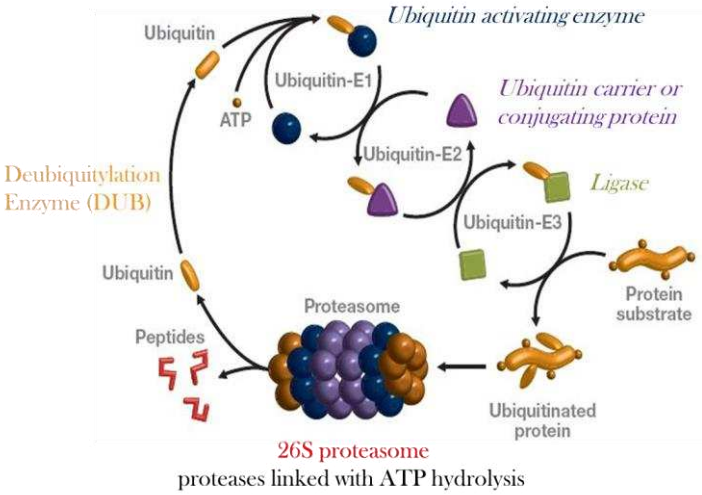

Figure 2.6 Representation of the ubiquitin-proteasome system. The ubiquitin-activating enzyme E1 activates ubiquitin through an ATP-dependent process. The activated ubiquitin is passed to a ubiquitin-conjugating enzyme E2 and finally passed to a E3 ubiquitin ligase. The substrate protein is recognized by the E3 ubiquitin ligase, allowing ubiquitin to be transferred to the substrate. The ubiquitinated protein gets degraded by the proteasome into peptides and deubiquitylation enzymes DUBs cleave off the ubiquitin units to be recycled.

DUBs, along with E1s, E2s, and E3s, form the ubiquitin-proteasome system (UPS), responsible for maintaining protein homeostasis and the constant levels of free ubiquitin. [35] Due to its complexity, determining the activity and specificity of the UPS under physiological conditions represents a major challenge. Mass spectrometry has become the standard method for quantifying protein levels in cells and tissues due to its high identification specificity, broad applicability in proteomics workflows, and high sensitivity. [36]

2.5. Enrichment of ubiquitylated peptides

The global analysis of protein ubiquitylation through mass spectrometry (MS) is commonly known as ubiquitinomics (or ubiquitomics/ubiquitylomics). Since ubiquitylation events are typically sub-stoichiometric, proteins or peptides that have been modified by ubiquitin need to be enriched before MS analysis, using protein-centric or peptide-centric methods. The di-Gly enrichment method, a peptide-centric ubiquitinomics, has been used to carry out the experiments. [37]

The di-Glycine peptide enrichment

The C-terminus of ubiquitin, which binds to the ε-amino group of a lysine residue on the target protein, contains a conserved sequence of two glycine residues followed by an arginine. The presence of the GG on the side chain of that lysine prevents cleavage by trypsin at that site. Thereby, when lysates are digested with trypsin, ubiquitylated proteins are cut into fragments that contain two glycine residues covalently linked to the lysine ε-amino group (**figure 2.7**). These Lys-ε-Gly-Gly (K-GG) peptides are enriched with monoclonal antibodies and identified by MS, due to a characteristic mass shift of 114.043 Da, corresponding to the -GG adduct, that distinguishes them from unmodified peptides. [38]

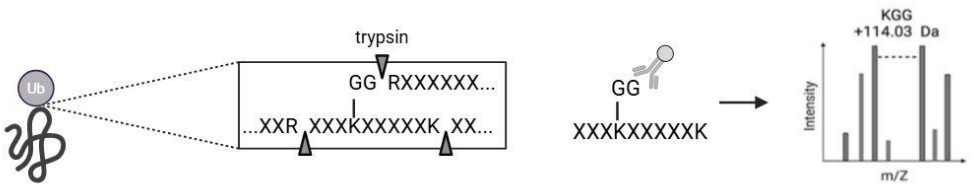

Figure 2.7 For MS-based K-GG remnant profiling, proteins are first digested with trypsin, breaking ubiquitylated proteins down into peptide fragments that contain modified lysine residues, in which two glycine residues are covalently linked to the lysine ε-amino group. These Lys-ε-Gly-Gly peptides are subsequently enriched with monoclonal antibodies and identified by MS, due to a characteristic mass shift of 114.043 Da, corresponding to the -GG adduct. (Modified from Steger et al., 2022)

The very first application that demonstrated K-GG peptide identification could reveal ubiquitylation sites genome-wide was a yeast study in 2003, and it catalogued 110 ubiquitylation sites. [39] Other groups applied overexpression of His-tagged ubiquitin for early mammalian works but, yielded relatively few K-GG peptides because the enrichment was performed at the protein level. [40], [41], [42] A breakthrough arrived in 2010 when Jaffrey and colleagues generated a monoclonal antibody that directly captures K-GG peptides from proteolytic protein digests, increasing the detectable sites to ~400 in cultured cells.[43] Subsequent large-scale profiling showed that chemical proteasome inhibition could uncover more than 20,000 ubiquitylation sites in mouse tissues. [44] However, a major problem of early K-GG peptide enrichment experiments was the requirement for very large protein amounts (20 mg or more). This changed when Carr et al. cross-linked the antibody to the affinity matrix and optimized protein input and antibody amount, enabling quantification of nearly 20,000 sites in SILAC* experiments with only 5 mg of protein.[45] Optimisations such as using multiplexed tandem mass tag (TMT) labeling, synchronous precursor selection MS^3 (SPS-MS^3) acquisition, and cartridge-based high pH reversed-phase peptide fractionation improved

* SILAC = Stable Isotope Labeling by Amino Acids in Cell Culture

throughput, data completeness and sensitivity. Even though potential batch effects, along with a high number of missing quantifications, may occur when larger sample numbers are processed. [46], [47]

Despite being the most widely used approach for studying ubiquitin signalling on a global level, MS-based K-GG remnant profiling has its limitations. First, monoclonal antibodies directed against K-GG peptides do not recognize -GG-modified protein N-termini. Moreover, by proteolytically cleaving ubiquitylated proteins, chain topology information gets lost. In addition, ISG15- and NEDD8-modified proteins also yield K-GG remnant peptides when cleaved by trypsin since their C-termini are homologous with ubiquitin (**figure 2.8**). Even if the number of K-GG sites linked to these modifications is minimal (<6%), they still have an impact on the identification of ubiquitination sites on a large scale, and therefore, complementary strategies (e.g., UbiSite, COFRADIC, WaLP) have been developed. [48], [49]

Blagoev and colleagues developed the UbiSite approach for the clear identification of ubiquitylation sites. This method relies on the enrichment of peptides using a specific antibody that targets a 13 amino acid residue remnant produced by LysC** digestion of ubiquitylated proteins. These peptides can either be directly quantified using mass spectrometry (MS) or undergo further cleavage with trypsin before MS analysis. In this case, due to LysC digestion, the peptide flow-through obtained after immunoprecipitation of K-GG peptides (derived from neddylated proteins) includes larger fragments that can be additionally cleaved by trypsin, followed by another round of K-GG peptide enrichment to isolate ubiquitylated substrates (**Figure 2.8**). [49]

** Lys-C is a protease that cleaves proteins on the C-terminal side of lysine residues.

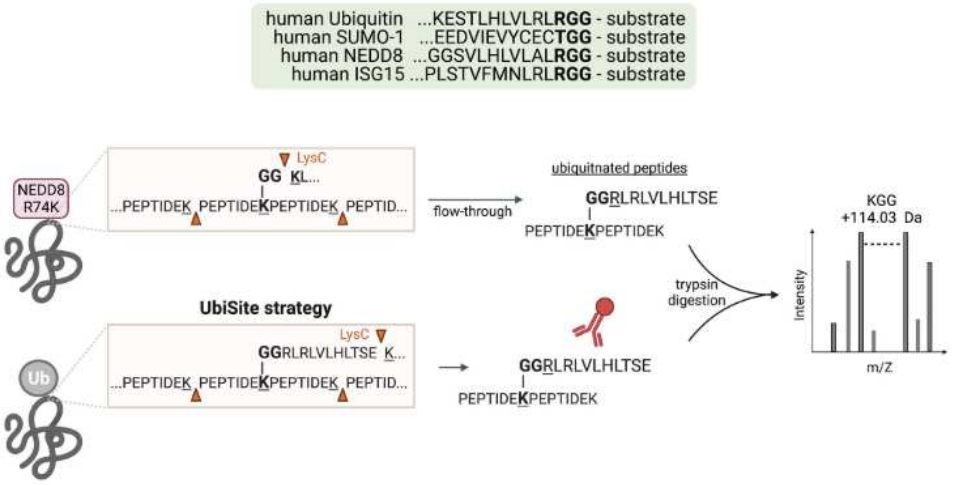

Figure 2.8 Strategy for mapping neddylation sites. NEDD8-R74K substitution combined with LysC digestion of proteins generates K-GG remnant peptides specific for NEDD8-modified proteins that can be captured using conventional K-GG antibodies. The flow-through can be collected and further digested with trypsin, generating ubiquitin-specific K-GG remnant peptides that can once again be captured using K-GG antibodies. UbiSite strategy for unambiguously identifying ubiquitylation sites: an antibody is used to enrich peptides harboring a 13 amino acid residue remnant generated by LysC digestion of ubiquitylated proteins. These peptides can be directly quantified by MS or further cleaved with trypsin prior to MS analysis. (Steger et al., 2022)

Since no specific diGly-enrichment–based protocol for the comprehensive study of ubiquitinomics was available in the literature, a tailored methodology was needed to enable effective analysis of ubiquitylated proteins to study LRRK2 mediated signalling in MEFs of wild-type and [D620N] VPS35. For more sensitive and reproducible results, the di-Gly antibody-based enrichment has been coupled with a data-independent acquisition (DIA) method. In contrast to data-dependent acquisition, DIA fragments all co-eluting peptide ions within specific mass-to-charge (m/z) windows and acquires them at the same time. This leads to more precise and accurate quantification with fewer missing values and higher identification rates over a larger range. [50], [51]

3. Aim of the work

This thesis aimed to investigate the molecular mechanisms linking alterations in LRRK2 kinase activity to proteasomal degradation in Parkinson's disease. It has been shown that the VPS35 [D620N] mutation, associated with familial Parkinson's disease, increases LRRK2 kinase activity and down-regulate the lysosomal protein content. Particularly, this mutation promotes the proteasomal degradation of RILPL1 after its recruitment to the lysosome.[30] However, the downstream effects of this hyperactivation on the ubiquitin-proteasome system remain poorly understood.

A primary object of the work was to determine how the ubiquitinome is altered in the presence of the [D620N] mutation and how these changes are modulated by pharmacological inhibition of LRRK2 kinase activity in mouse embryonic fibroblasts (MEFs) expressing either wild-type (WT) or D620N-mutant VPS35.

To address this, a global ubiquitinomics methodology based on di-Gly (K-ε-GG) peptide enrichment was developed and optimized. This method enabled the identification and quantification of ubiquitination events at specific sites across the proteome.

By combining this proteomics approach with genetic and pharmacological models, this study aimed to provide novel insights into the interactions between LRRK2 kinase activity and the ubiquitin-proteasome system in the presence of a VPS35 mutation. Ultimately, these findings may contribute to a better understanding of the molecular pathology of Parkinson's disease and potentially lead to new therapeutic strategies targeting these pathways.

4. Materials and Methods

4.1. Materials and reagents

Antibodies for biochemical studies

The following primary antibodies were used: 1:10000 α-Tubulin (Cell Signaling Technology); 1:10000 phospho-S935 LRRK2 (MRC PPU Reagents and Services); 0.1 µg/ml UDD2 10(12) (University of Dundee) (AB_2921228); 0.1 µg/ml LRRK2 Total C-terminal N241A/34 (AB_2877351); 0.1 µg/ml Rab10 Total (Nanotools) 0680-100 / Rab10-605B11 (AB_2921226); 1:10000 phospho-T73 Rab10 (Abcam); 1:5000 VPS35 StressMarq SMC-602 (AB_2820301); 1:10000 RILPL1 (Abcam). The secondary antibodies used were: 1:25000 IRDye 800CW Goat anti-Rabbit IgG LI-COR 926-32211 (AB_621843); 1:25000 (v/v) IRDye 680CW Goat anti-Mouse IgG LI-COR 926-68070 (AB_10956588).

4.2. Cell culture and MLi-2 treatment

Wild-type and homozygous VPS35[D620N] knock-in mouse embryonic fibroblasts (MEFs) were cultured in Dulbecco's Modified Eagle Medium enriched with 10% (v/v) fetal bovine serum (FBS), 2 mM L-glutamine, penicillin (100 U/ml), and streptomycin (100 µg/ml) supplemented with 1X nonessential amino acid solution and 1 mM sodium pyruvate. All cells were grown at 37°C with 5% CO2 in a humidified atmosphere. Both WT and VPS35 [D620N] cells were maintained in a 15cm dish to a ~80% confluency, and when required, they were treated with 200nM MLi-2 for 60 minutes.

4.3. Whole cell lysate preparation

To establish a di-Gly based global ubiquitinome methodology, the first thing to do was to test different lysis buffers and assess which one was more suitable for studying LRRK2 regulated ubiquitinome. The chosen lysis buffers were composed of:

- 8 M urea, 1mM ethylenediaminetetraacetic acid (EDTA), 1 mM 2-chloroacetamide (CAA), 150 mM sodium chloride (NaCl), 50 mM Tris-HCl pH 8, 10 μg/ml leupeptin, 1 mM phenylmethylsulfonyl fluoride (PMSF), one protease inhibitor cocktail tablet per 10ml (Roche), one PhosSTOP tablet per 10ml (Roche)
- 2% (by mass) sodium dodecyl sulfate (SDS) in 50 mM Tris HCl pH 8, 40mM CAA, 10 mM Tris(2-carboxyethyl)phosphine (TCEP), one protease inhibitor cocktail tablet per 10ml (Roche), one PhosSTOP tablet per 10ml (Roche)
- 1% sodium deoxycholate (SDC), 10 mM TCEP, 40 mM CAA, 75 mM Tris-HCl pH 8,5, one protease inhibitor cocktail tablet per 10ml (Roche), one PhosSTOP tablet per 10ml (Roche)

For each lysis buffer used, cell lysates were prepared using a different workflow as described in **figure 4.1**.

Preparation of cell lysates in 8 M urea lysis buffer

Both WT and VPS35 [D620N] cells, when at 80% confluency, were washed three times with ice-cold PBS (phosphate-buffered saline) to eliminate all the cell culture media. After this, 500 μl of ice-cold urea-based lysis buffer (recipe above) was added to each dish and kept on ice for 20 min. Subsequently, cells were scraped and collected in low-binding tubes using non-autoclaved tips and sonicated using a Bioruptor device at 4°C for 15 cycles, 30 sec on and 30 sec off. After sonication, samples were centrifuged at 4°C, 21,100 g (or maximum speed) for 15 min. Supernatants were transferred into new tubes and 10 μl per

sample was aliquoted for the BCA (bicinchoninic acid) protein amount estimation assay.

Preparation of cell lysates in 2% SDS lysis buffer

Cells were washed and lysed following the procedure previously described, with the exception that 500 µl of 2% SDS lysis buffer were used for each dish. After lysis, samples were boiled at 95°C for 5 min and sonicated (Bioruptor device, 15 cycles, 30 sec on / 30 sec off). Due to DNA aggregation, cell lysates in SDS needed to be sonicated at a lower frequency using a probe. Protein lysates were clarified by centrifugation at 21,100 g for 15 min and protein amount was estimated through BCA assay.

Preparation of cell lysates in 1% SDC lysis buffer

Cells were washed and lysed in 500 µl of 1% SDC lysis buffer. Lysates were boiled at 95 °C for 10 min, sonicated using a Bioruptor (15 cycles; 30 sec on / 30 s off), and centrifuged to collect supernatants. Protein concentration was determined by BCA assay.

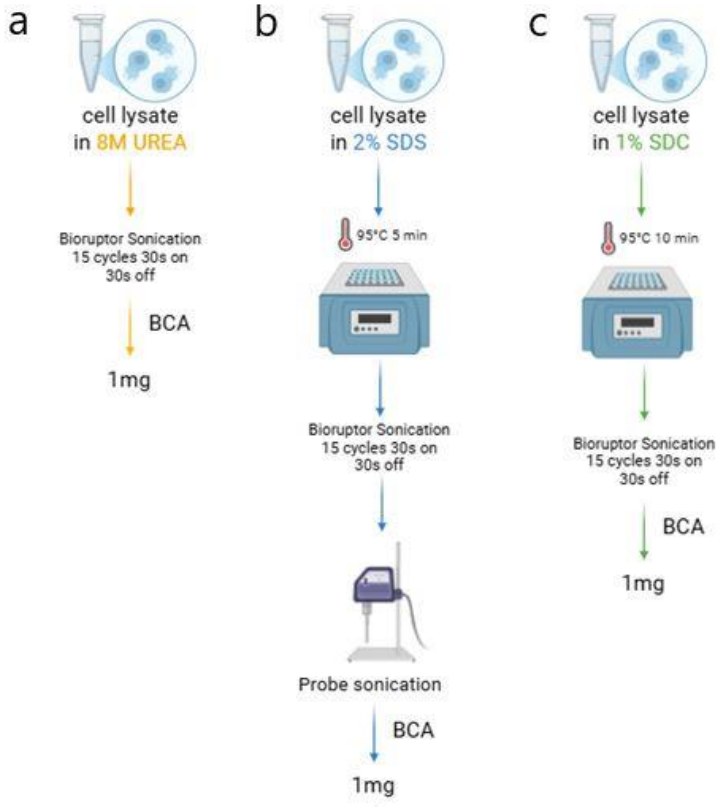

Figure 4.1 Workflow of cell lysate preparation. (a) Cell lysates in urea get sonicated at 4°C for 15 cycles 30 seconds off and 30 seconds on. (b) Cell lysates in SDS were boiled at 95°C for 5 minutes prior to sonication at the same conditions as in (a). In addition, SDS lysates were sonicated again at lower frequency. (c) Cell lysates in SDC were boiled for 10 minutes at 95°C before sonication as in (a) and (b). Finally, all lysates were quantified through BCA assay and 1 mg were aliquoted.

4.4. Quantitative immunoblotting analysis

Western blot analysis was conducted whenever cells were treated with MLi-2 to assess its effectiveness.

Polyacrylamide gels were self-casted as follows:

- Stacking gel: 4% (w/v) acrylamide, 0.125 M Tris-HCl (pH 6.8), 0.1% (v/v) SDS, 0.1% (v/v) Tetramethylethylenediamine (TEMED), and 0.08% (w/v) Ammonium persulfate (APS).
- 10% Bis-Tris running gel: 10% (w/v) acrylamide, 0.375 M Bis-Tris (pH 6.7), 0.1% (v/v) SDS, 0.08% (v/v) TEMED, and 0.05% (w/v) APS.

Twenty micrograms of each lysate were loaded onto the self-cast gel and separated by electrophoresis at 120 V for 2 h using NuPAGE MOPS SDS running buffer. Proteins were subsequently transferred onto 0.45 µm nitrocellulose membranes at 90 V for 90 min on ice in transfer buffer (48 mM Tris, 39 mM glycine, and 20% (v/v) methanol). Successful protein transfer was verified by brief Ponceau S staining, followed by washing with Elix water. Stained membranes were imaged using a ChemiDoc MP Imaging System (Bio-Rad), and residual dye was removed with TBS-T (50 mM Tris base, 150 mM NaCl, and 0.1% (v/v) Tween-20).

Membranes were blocked with 5% (w/v) skimmed milk in TBS-T for 1 h at room temperature, then washed three times with TBS-T and incubated with primary antibodies overnight at 4°C. Once primary antibodies were removed, membranes were washed three times in TBS-T and were incubated with secondary antibodies for 1 h at room temperature, followed by three additional washes (10 min each) in TBS-T. Protein detection was performed by near-

infrared fluorescence using an Odyssey CLx imaging system, and band intensities were quantified with Image Studio Lite software.

4.5. Digestion of cell lysates

Following cell lysis, proteins were digested with trypsin. Sample processing workflows varied according to the composition of the lysis buffer, as shown in **figure 4.2**.

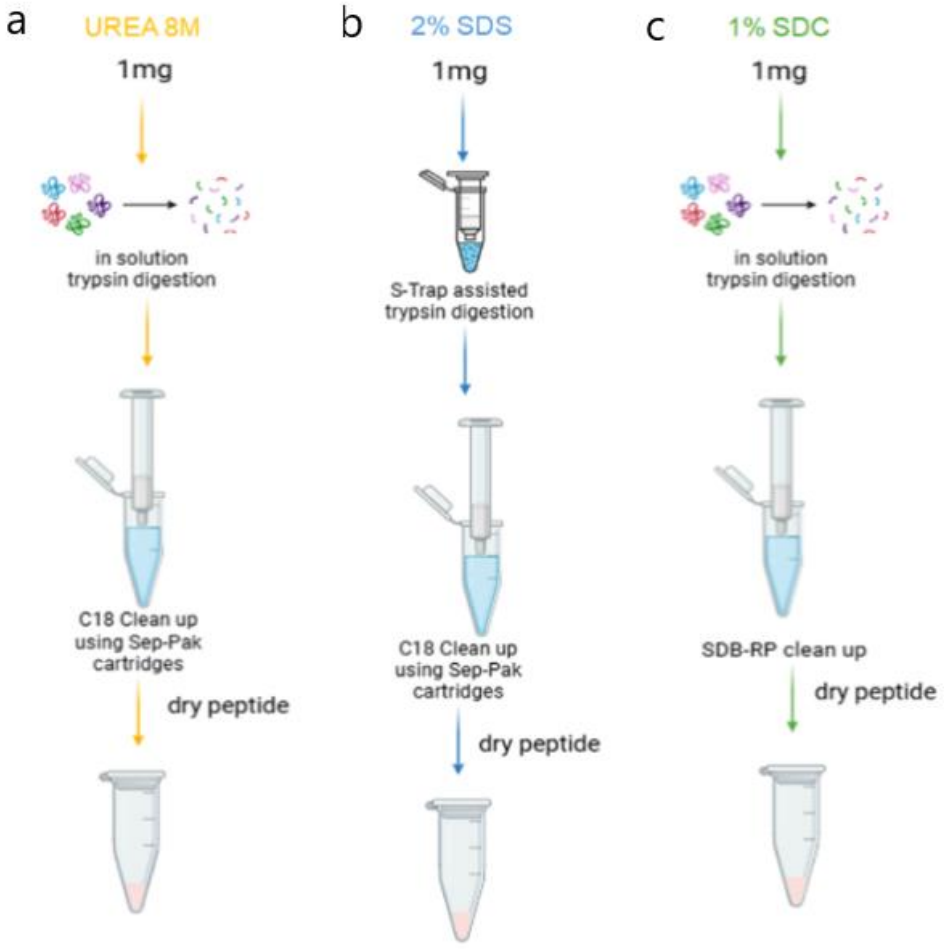

Figure 4.2 Workflow of trypsin protein digestion. (a) 1 mg of urea-lysed cell extract was aliquoted and subjected to in-solution trypsin digestion. The resulting peptide mixture was purified using C18 cartridges and subsequently dried. (b) 1mg of SDS-lysed cell extract was aliquoted and digested using S-Trap columns. The digest was purified using C18 cartridges

and peptides were dried. (c) Same amount of SDC lysate was digested as in (a) and purified through SDB-RP solid phase extraction. Peptides were also dried.

In-solution Trypsin digestion of urea- and SDC-based cell lysates

In-solution trypsin digestion was carried out on cell lysate samples equivalent to 1 mg of total protein, as determined by BCA assay. Reduction of samples was performed by adding 5mM of a solution of 50mM TCEP dissolved in 300 mM TEABC (Triethylammonium bicarbonate pH 8.5). After reduction, samples in urea were incubated at room temperature for 1h with a gentle agitation of 1200 rpm, while those containing SDC were incubated at 60 °C, 1200 rpm for 30min. Samples were alkylated by adding 20mM chloroacetamide and incubated again under the same conditions. Before the digestion step, samples containing urea were transferred into 15ml tubes and diluted with 1M Tris-HCl pH 8,5, to bring 8M urea to a final concentration of 1.5 M.

Finally, digestion was performed by adding a 1:100 dilution of Trypsin /Lys-C Protease MS-Grade dissolved in 50mM TEABC and a 1:20 dilution of trypsin from bovine pancreas dissolved in 0.05% acetic acid. Samples were incubated overnight on a Thermomixer at 1200 rpm at room temperature (at 37°C for SDC samples).

S-TRAP ™ assisted Trypsin digestion of SDS-based cell lysates

S-Trap-assisted trypsin digestion was performed on SDS-based cell lysate samples corresponding to 1 mg of total protein (**figure 4.3**). Reduction was carried out by adding 5 mM TCEP prepared in 300 mM TEABC, followed by incubation on a thermomixer at 60 °C for 30 min at 1250 rpm. Alkylation was then performed by adding 40 mM CAA, and samples were incubated under the same conditions. The initial SDS concentration in the samples was 2% (v/v), which was subsequently increased to a final concentration of 5% (v/v). Samples were acidified to 1% (v/v) TFA, and, due to the increased volume, transferred into 15 ml tubes. Subsequently, six volumes of S-Trap binding buffer (90% methanol, 100 mM TEAB, pH 7.1) were added to each sample. S-Trap ™ midi columns (ProtiFi) were used to carry out the digestion. Samples were loaded onto the columns and spun at room temperature at 2500g for 2

min. Flow through was discarded and the columns were washed with S-Trap binding buffer (~3ml) a total of four times. To make sure that everything eluted from the column, another empty spin was given at 3800g for 2 min. Flow through was discarded and columns were transferred into new 15 ml tubes. Thereafter, samples were digested using 1:100 dilution of Trypsin/Lys-C Protease MS-Grade dissolved in 50 mM TEAB pH 8 and a 1:15 dilution of trypsin from bovine pancreas dissolved in 0.05% acetic acid. Tubes were briefly spun at 0,2 g for 1 min and eluates were reapplied back onto the columns. Samples were left on a Thermomixer firstly for one and a half hour at 47°C with no shaking, and then at room temperature overnight. Peptides were eluted with:

- 500 µl of 50 mM TEAB dissolved in LC water and spin at 1250 rpm for 2 min;
- 500 µl of 0.2% (v/v) formic acid (FA) in LC water and spin at 1250 rpm for 2 min;
- 500 µl of 0.2% (v/v) FA in 50% (v/v) ACN, three times in total. Firstly, spun at 1250 g for 2 min, then 2000g for 5 min, and lastly at 2500 g for 5 min plus another empty spin at 3800 g for 10 min;

Once peptides were complicatedly eluted from the column, those were discarded, and eluates were centrifuged at 3800 g for 10 min. Supernatants were collected in 2ml low-binding tubes and froze in dry ice prior to drying the solvent using a Speed-Vac system.

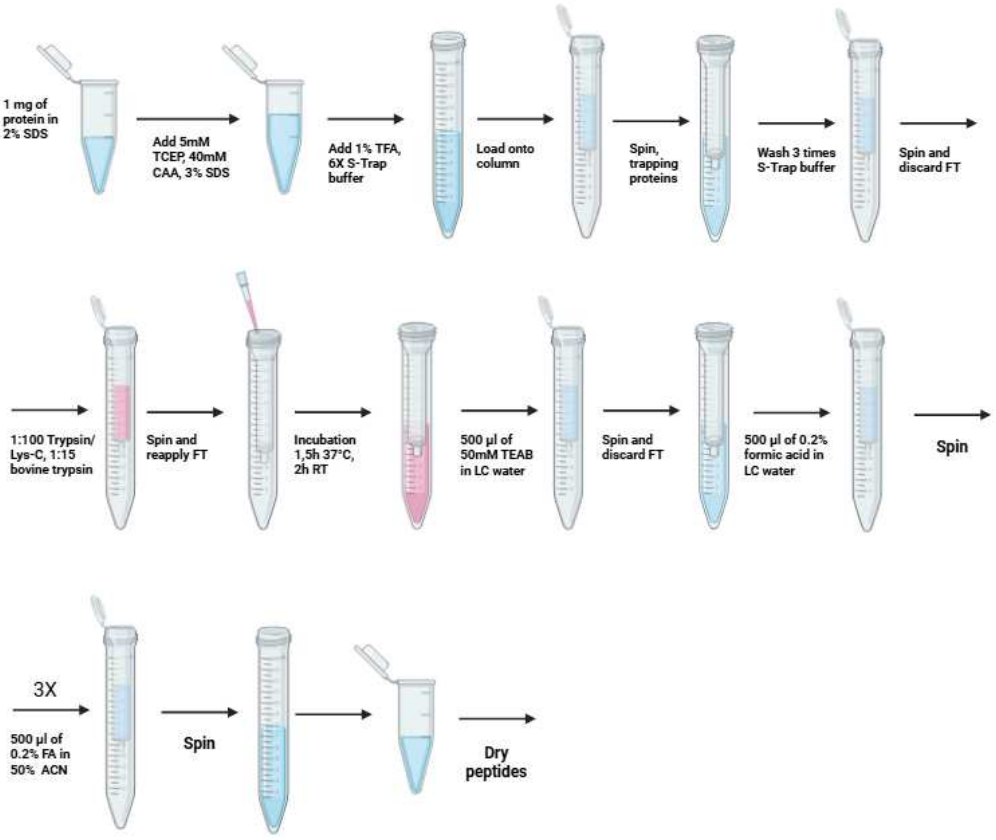

Figure 4.3 Trypsin digestion of cell lysates in 2% SDS using S-Trap midi columns (ProtiFi). 1mg of protein lysate was reduced and alkylated by adding 5mM TCEP and 40mM CAA, respectively. Then samples were acidified and diluted by adding 1% (v/v) TFA and 6X S-Trap binding buffer, respectively, and loaded onto the corresponding midi column. Once proteins were trapped onto the stationary phase, the columns were washed with S-Trap binding buffer a total of four times, spinning in between each wash. Flow-through was discarded and trypsin was added onto the columns. Tubes were spun, and the trypsinized flow-through was reapplied onto the column. Samples were incubated at 47°C for 1,5h with no agitation and then at room temperature overnight or at least for 2 hours. After the digestion, peptides were eluted using 500 µl of 50 mM TEAB in LC water, 500 µl of 0.2% (v/v) formic acid in LC water, three times with 500 µl of 0.2% (v/v) formic acid in 50% (v/v) acetonitrile, spinning between each step. Eluates were centrifuged for 10min at 3800 g, and supernatants were dried using a SpeedVac system.

C18 clean-up of urea- and SDS-based protein digests

Samples containing either Urea or SDS were prepared prior to C18 clean up. Urea-containing lysates were acidified by adding 1% (v/v) of trifluoroacetic acid (TFA) prepared in LC–MS grade water. The samples were centrifuged at

4 °C for 10 min at 4000 rpm so that trypsin could precipitate. The supernatant was collected for C18 cleanup. C18 cartridges were pre-assembled into 15 mL Falcon tubes to facilitate sample loading.
Lyophilized peptide pellets derived from S-Trap assisted digestion of SDS samples were reconstituted in 1% (v/v) of TFA in LC–MS grade water. Samples were incubated on a thermomixer at room temperature at 1800 rpm for 30 min to ensure complete solubilization prior to cleanup.

C18 solid-phase extraction of protein digests was performed using Sep-Pak Vac 1cc (50 mg) tC18-Cartridges (Waters) as follows:

- Activation of the cartridge: 1 ml 100% acetonitrile (ACN) + centrifuged at 1000 rpm for 1 min. Repeated three times and flow through was discarded.
- Equilibration of the cartridge: 1ml sol A (0,1% TFA, 90% ACN) + centrifuged at 1000 rpm for 1 min. Repeated a total of five times and flow through was discarded.
- Loading: the sample was loaded on the cartridge and allowed to pass through it by gravity. The flow through was collected and reapplied on the cartridge.
- Washing: 1ml sol A + centrifuged at 1000 rpm for 1 min. Repeated a total of four times and flow through was discarded.
- Elution: 350 µl of sol B (0,1% TFA, 50% ACN) + centrifuged at 1000 rpm for 1 min. The flow through was collected in a clean low binding tube.

Following the clean-up, samples were vacuum-dried using a Speed Vac system and stored at -20°C until di-Gly peptide enrichment.

SDB-RP clean-up of SDC-based digests

Digests containing 1% SDC were desalted using 1ml Strata-X-C cartridges placed in 15ml tubes. Samples were diluted with twice their volume of wash buffer I (1% TFA (v/v) and 99% ethyl acetate). Cartridges were conditioned three times with 1 ml of isopropanol, and another three times with 1 ml of

elution buffer (5% (v/v) NH_4OH, 80% acetonitrile), each wash followed by centrifugation at 1000 rpm for 1 min. Equilibration was performed six times with 1 ml of wash buffer I and centrifuged at same conditions. Then, samples were loaded onto the cartridges, let it pass through by gravity and reapplied back on. After loading, the cartridges were washed six times with 1 ml of wash buffer I and three times with 1 ml of wash buffer II (0.2% (v/v) TFA in LC water), spinning at 1000 rpm for 1 min after each wash. Elution was carried out six times with 1 ml of elution buffer. The first 2 ml were allowed to flow through by gravity, while the remaining 4 ml were centrifuged at 1000 rpm for 1 min. Eluates were collected in 15 ml tubes and labelled accordingly. Samples were snap-frozen in liquid nitrogen, lyophilized, and stored at -20°C until di-Gly peptide enrichment.

4.6. Di-Gly peptide enrichment and C18 Stage-tip clean up

Di-Gly peptide enrichment of protein digests

Di-Gly remnant containing peptides were enriched using the PTMScan® Ubiquitin Remnant Motif (K-ε-GG) Kit (Cell Signaling Technology). One mg of peptide material was used for di-Gly peptide enrichments. First, lyophilized peptides were resuspended in 700 µl of immunoaffinity purification (IAP) binding buffer (contains 5% acetonitrile) and shaken gently (1800 g) at room temperature for 30 min using a thermomixer to ensure complete solubilization. After dissolving the peptides, solutions were cleared by centrifugation at 21,100 g for 5 min. When present, small, insoluble pellets were discarded and supernatants were transferred to clean low binding tubes. To check that samples had a basic pH, a small volume was spotted on a pH indicator paper. If necessary, 1M Tris-HCl pH 8.0 was added to the solution until basic. In the meantime, 5 µl per sample of PTMScan® HS K-ε-GG remnant magnetic immunoaffinity beads were equilibrated three times with 450 µl cold PTMScan HS IAP bind buffer (1X), followed by a brief spin at 1,000 g for 5 seconds to

bring down any buffer clinging to the cap and the sides of the tube. Between each wash, flow-through was discarded using a magnetic rack to trap the beads. After the last wash, flow-through was discarded and of cold 1X PTMScan® HS IAP bind buffer (count 10 µl/ sample) was added to the beads pipetting gently to obtain a uniform suspension. To ensure reproducible results, an equal 10 µl of the antibody-beads suspension was added to each peptide solution previously prepared, tubes were sealed with parafilm and placed on an end-to-end rotator at 4°C for a 2-hour incubation.

Thereafter, tubes were spun at 1,500 g for 1 min and using a magnetic rack, solutions containing unbound peptides were transferred to clean low binding tubes. The remaining beads were washed a total of three times with 500 µl of cold PTMScan® HS IAP bind buffer (1X), mixed by inverting the tube twenty times and briefly centrifuged at 1,500 g for 1 min. Beads were also washed twice with 500 µl of LC MS grade water and briefly spun at 1,500 g for 1 min. Afterwards, peptides of interest were eluted twice with 50 µl of 0.2% (v/v) TFA in LC water and incubated on a thermomixer at 1250 rpm for 10 min.

C18 Stage-tip clean-up of di-Gly enriched peptides

Following elution, di-Gly peptide enriched samples were desalted using homemade C18 stage tips assembled punching two C18 layers using a 16-gauge needle and pushing them into a 200 µl tip. The tips were staged into 1.5 ml tubes using PTFE-O rings. The C18 resin was activated twice by adding 80 µl of 100% acetonitrile and equilibrated twice with 80 µl of 0.1% (v/v) TFA in LC water. For each step, the according solution was added to the tip and passed through by centrifugation. Di-Gly enriched samples were loaded onto the stationary phase and tubes were spun for 2 min at 1,500 g at room temperature. To make sure that all the peptides of interest would bind to the resin, the flow through was reapplied onto the stage-tips and spun again. Thereafter, peptides were washed with 80 µl of 0.1% (v/v) TFA in LC water a total of two times followed by centrifugation for 3 min at 2,000 g, verifying that the solution passed through. Eventually, peptides were directly eluted twice with 30 µl

0.1% (v/v) TFA in 50% ACN into clean low binding tubes, snap frozen and dried using a Speed-Vac system.

4.7. Mass Spectrometry Analysis

Preparation of di-Gly enriched samples for LC/MS-MS injection

After the di-Gly peptide enrichment and C18 clean-up, dried peptides were reconstituted in of Astral LC buffer (0.1% (v/v) formic acid in 3% ACN and 0.015% Ndodecyl-ß-D-maltoside (DDM) in LC-grade water) and incubated on a Thermomixer for 30 min at 1800 rpm. Tubes were given a brief spin and protein content was checked using a Nano Drop system prior to LC/MS-MS analysis (1/3rd of the digest was transferred to a LC plate and injected). Samples were analysed using State-of-the-art Orbitrap Astral mass spectrometer interfaced with Vanquish-Neo liquid chromatography system. Peptides were loaded on 2cm trap column and resolved on a 15cm analytical column. The data was acquired using 40 sample per day LC method comprising of a total data acquisition of 30 min. The mass spectrometry data was acquired in a narrow-window data independent acquisition (DIA). The full MS scans were acquired at 240,000 resolutions in the scan range (m/z) of 380-980 and measured using ultra-high filed Orbitrap mass analyser. The DIA scans with isolation window of 4m/z comprising a total of 149 scans were acquired in the scan range (m/z) of 150-2000 and fragmented using normalised 25% HCD (Higher-energy collisional dissociation) and acquired using Astral mass analyser. The MS1 and DIA automatic gain control (AGC) targets were set to 500% and total ion injection accumulation times were set to 5ms and 3ms respectively. The total duty cycle was operated for 0.6 sec.

Total Proteome analysis

From trypsin digest samples 100 µl of the total 1100 µl were aliquoted for total proteome analysis and dried using a Speed-Vac system. Dried peptides were reconstituted in 240 µl of Astral LC buffer (final protein concentration of 0.375 µg/µl). Samples were incubated on a Thermomixer for 30 min at 1800 rpm

room temperature. Then, tubes were given a brief spin at maximum speed for 1 min and protein content was quantified using a Nano Drop system. 200ng of peptide amount was injected for DIA analysis using the same LC and mass spectrometer method described above.

DIA-NN data search

The DIA MS experiment's raw data for di-Gly enriched samples and total proteome was analyzed through DIA-NN 1.8.1 software using the default closed search workflow and searched against Mouse UniProt database. [52] Trypsin/Lys-C was selected as the digestive enzyme, and up to two missed cleavages were allowed. Carbamidomethylation at cysteine residue was considered as a fixed modification and oxidation at methionine residue was considered as a variable modification.

For di-Gly dataset search, GlyGly modification (+114.0429 Da) was also set as a variable modification. The precursor, peptide and protein group FDR was set at 1%. The output files were further processed for downstream statistical analysis using Perseus software suite (RRID:SCR_015753, version 1.6.0.15; https://maxquant.org/perseus/).[53] di-Gly sites table was filtered to have <70% of data completeness and missing values were imputed using normal distribution with a width of 0.3 and downshift value of 1.8. A Student's t-test was conducted comparing WT and D620N DMSO (negative control), as well as WT DMSO with MLi-2, and D620N DMSO with MLi-2. The text files from Perseus were subsequently imported into an in-house software, Curtain 2.0 (RRID: SCR_024465), for data visualization. [54]

Statistical analysis of immunoblots

Statistical evaluation of the immunoblotting analysis was conducted using GraphPad Prism (RRID:SCR_002798, version 9.3.1; http://graphpad.com/). A two-tailed unpaired T test was used to compare the statistics between WT and VPS35 [D620N]. One-way analysis of variance (ANOVA) was employed for comparing statistical data from more groups (WT DMSO, WT MLi-2, D620N DMSO, D620N MLi-2).

5. Results

5.1. Establishment of a di-Gly based global ubiquitinome methodology

To study the impact of LRRK2 on the ubiquitinome in VPS35 [D620N] MEFs, a new methodology has been developed. Homozygous VPS35 [D620N] knock-in mouse embryonic fibroblasts (MEFs) were cultured and lysed with three different methods (8M urea, 2% SDS, 1% SDC). Samples were processed in different ways accordingly to the lysis buffer used, as described in the methods' section. The three different extraction methods tested were compared based on the number of di-Gly sites detected. Data-independent acquisition (DIA) MS with equal protein amounts of whole-cell lysates from VPS35 [D620N] MEFs was undertaken, with three replicates per lysis condition. Over a total of 51.180 peptides analyzed, 29.308 had been modified with ubiquitin (57,27 %). MS data were searched through DIA-NN and further analyzed using Perseus software. Urea enabled the identification of the greatest quantity of di-Gly sites, approximately 25,000, while SDS followed with around 24,000, and SDC had close to 18,000 (**figure 5.1*a***). Data suggests that the urea-based extraction provides higher peptide recovery for ubiquitinomics analysis. The abundance rank plot illustrates how quantified proteins are distributed across all samples. The most prevalent proteins are those linked to the LRRK2 signaling pathway and various Parkinson's disease related genes (**figure 5.1*b***). The data demonstrate that LRRK2 and TMEM55B are consistently detected across a wide range of abundances, indicating reliable quantification of biologically relevant targets within the proteome dataset. The principal component analysis (PCA) of measured di-Gly sites across various lysis conditions reveals that urea replicates are closely grouped, whereas SDS and

SDC create distinct clusters, reflecting the influence of lysis chemistry on protein extraction and downstream peptide identification (**figure 5.1*c***).

Even though urea yielded the highest recovery rate of di-Gly sites, SDS provided better solubilization and enabled greater membrane protein coverage, making it more suitable for comprehensive ubiquitinome profiling in complex biological samples. In addition, the workflow is straightforward and still gives a comparable recovery rate. For these reasons, SDS was chosen as the most suitable lysis buffer for studying how LRRK2 activity influences the ubiquitinome system in WT and VPS35 [D620N] MEFs.

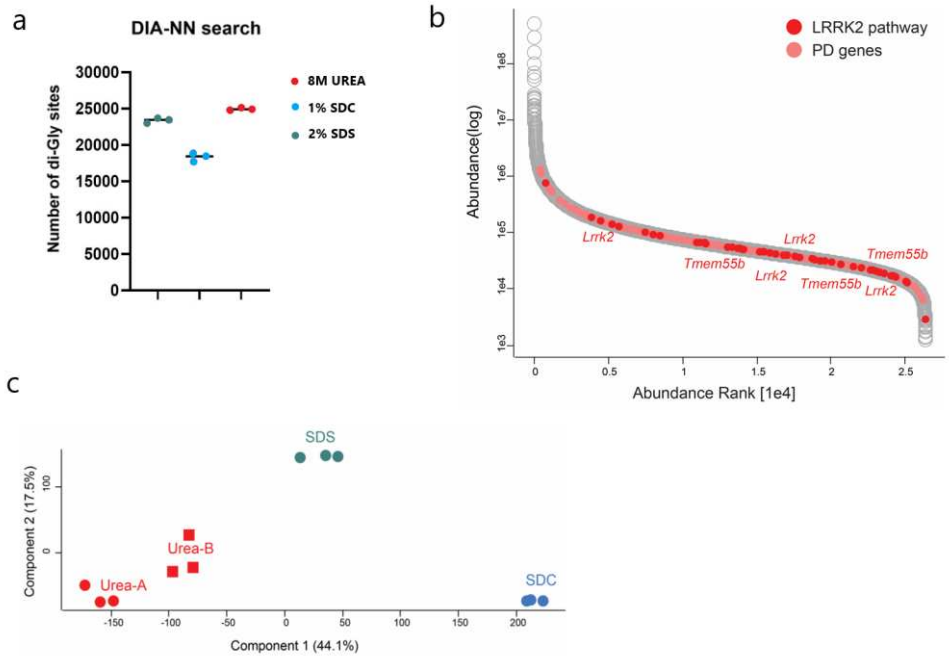

Figure 5.1 Results summary for different extraction methods in VPS35 [D620N] MEFs with three technical replicates per condition. (a) The number of identified di-Gly sites obtained from DIA-NN searches under three different lysis conditions: 8M urea (in red), 2% SDS (in green), and 1% SDC (in blue). Urea yielded the highest number of di-Gly site identifications (~25,000), followed by SDS (~24,000) and SDC (~18,000). Each point represents an independent replicate. (b) Abundance rank plot showing the distribution of quantified proteins across all samples. Proteins associated with the LRRK2 signalling pathway are indicated in red and other PD-related genes in pink. (c) Principal component analysis (PCA) across all lysis conditions. Urea replicates cluster closely together, while SDS and SDC form separate clusters, indicating clear differences in the proteomic profiles obtained from each condition.

5.2. Defining LRRK2 regulated ubiquitinome

The developed di-Gly-based methodology was used to define how LRRK2 regulates the ubiquitinome. Wild-type and homozygous VPS35 [D620N] knock-in MEFs were cultured and treated with 200nM MLi-2 for 1h prior to lysis. Cells were lysed in 2% SDS lysis buffer and samples were further processed as described in the methods' section. Briefly, proteins were digested with trypsin/Lys-C using S-Trap columns and purified through C18 clean-up. Digests were subjected to di-Gly peptide enrichment while a small aliquot was used for total proteome analysis.

Immunoblot analysis of lysates confirmed literature data that the VPS35 [D620N] mutation enhanced LRRK2-mediated Rab10 phosphorylation about 4-fold, which drastically dropped when using MLi-2. On the other hand, RILPL1 levels decrease in the mutant compared to WT levels, although no significant effect is shown when treating with MLi-2 (**figure 5.2**).

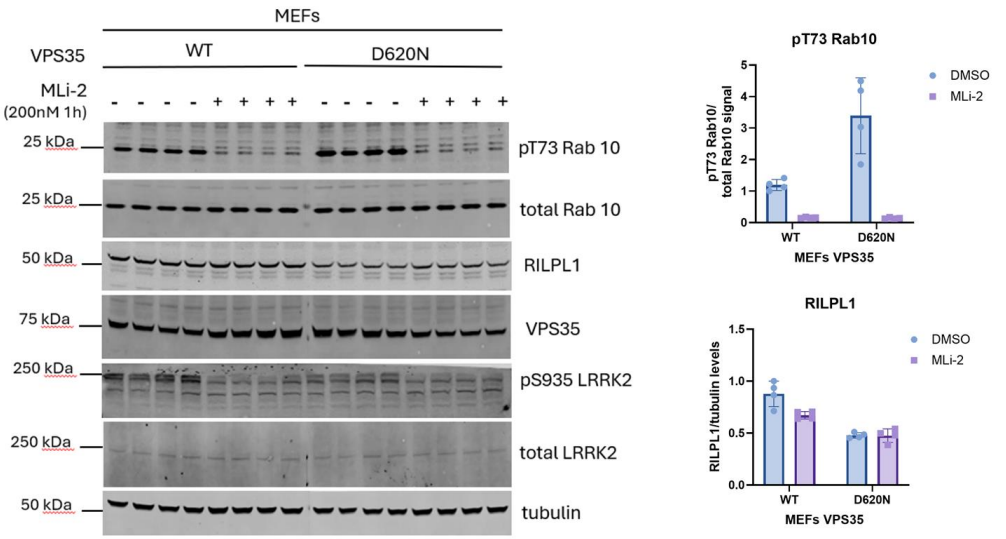

*Figure 5.2 Results of immunoblot analysis. Before lysis, WT and VPS35 D620N MEFs were treated for 1 hour with 200nM MLi-2 as a LRRK2 inhibitor or DMSO as a negative control. Twenty micrograms of whole cell lysate (in 2% SDS) was subjected to immunoblot analysis using the LI-COR Odyssey CLx Western blot imaging and the indicated antibodies. Each lane indicates a sample derived from a different dish of cells. Quantitation of immunoblotting data is shown as mean ± SEM. Data were analyzed using two-tailed unpaired t test (**P < 0.01,***P < 0.001, and ****P < 0.001).*

Analysis of WT and VPS35 [D620N] ubiquitinome

Both WT and VPS35 [D620N] trypsin digests underwent di-Gly enrichment of ubiquitylated peptides. Samples were then purified and injected on an Orbitrap Astral mass spectrometer. DIA MS data were searched through DIA-NN software, analyzed using Perseus and visualized on Curtain, related web links are provided in the figure descriptions. The overall distinct di-Gly sites detected were about 25,000 for WT and around 28,000 sites for the mutant. Between DMSO and MLi-2, no substantial differences were noted within each group (**figure 5.3*a***). Sample preparation and data collection were proved to be reliable through Pearson correlation analysis. High correlation values ($r > 0.9$) among replicates demonstrate the reproducibility of the method within each condition and the consistency in the results obtained from the DIA-NN search. (**figure 5.3*b***). The efficiency of the trypsin/Lys-C digestion was assessed in terms of percentages of missed cleavage in the total proteome analysis (**figure 5.3*c***). Most peptides showed complete cleavage (>80% of zero missed

cleavages), while a smaller number had one or two missed cleavage sites (fewer than 20%). Similar distribution across all experimental conditions demonstrates high digestion efficiency and comparable sample processing quality.

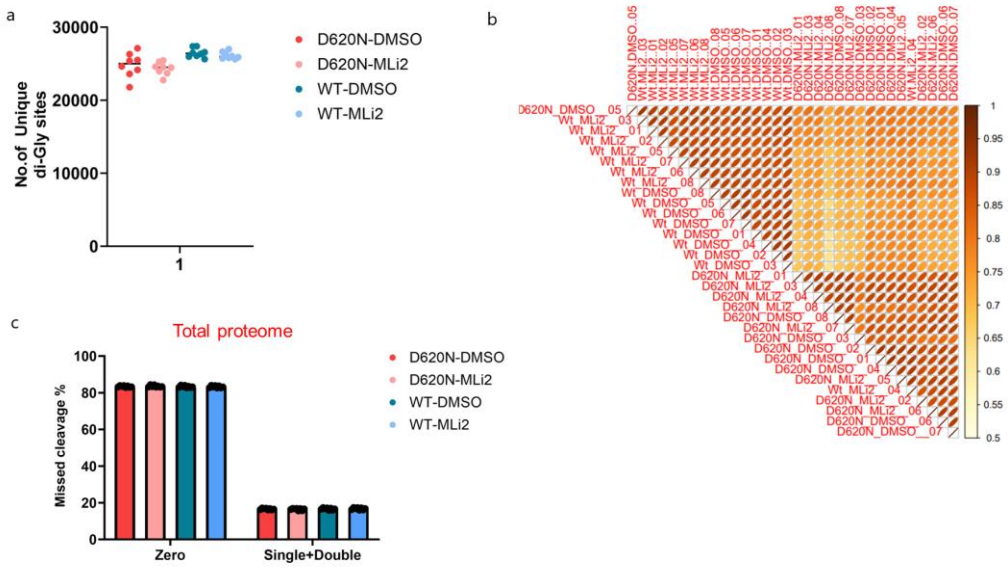

Figure 5.3 Results summary of ubiquitinome analysis of di-Gly enriched WT and VPS35 [D620N] ± MLi-2 MEFs. (a) The total number of unique di-Gly sites identified across experimental conditions. Both WT DMSO (in green) and WT MLi-2 (in light blue) and VPS35 [D620N] DMSO (in red) and MLi-2 (in pink) samples were analyzed, ranging approximately 25,000 sites for WT and 28,000 sites for the mutant. No significant change was observed between DMSO and MLi-2 within each group. Each point represents an independent replicate with 8 replicates per condition. (b) Pairwise Pearson correlation heatmap highlighting the reproducibility among biological replicates within each condition. High correlation coefficients (r > 0.9) between replicates indicate a strong level of consistency in the DIA-NN search results. (c) Distribution of missed cleavage percentages in the total proteome analysis. Most peptides were fully cleaved (>80% of zero missed cleavages), while a smaller proportion exhibited one or two missed cleavage sites (less than 20%).

Principal Component Analysis (PCA) on Perseus software enabled the visualization of the ubiquitinome profiles for each replicate across the four experimental conditions (**figure 5.4**). Analysis revealed two potential outliers, WT MLi-2 #4 and [D620N] DMSO #5, displaying distinct clustering patterns

compared to the other replicates in their respective groups (**figure 5.4*a***). This might be due to a swap of samples during the di-Gly enrichment step. The analysis was conducted again excluding those two in order to achieve more accurate results (**figure 5.4*b***).

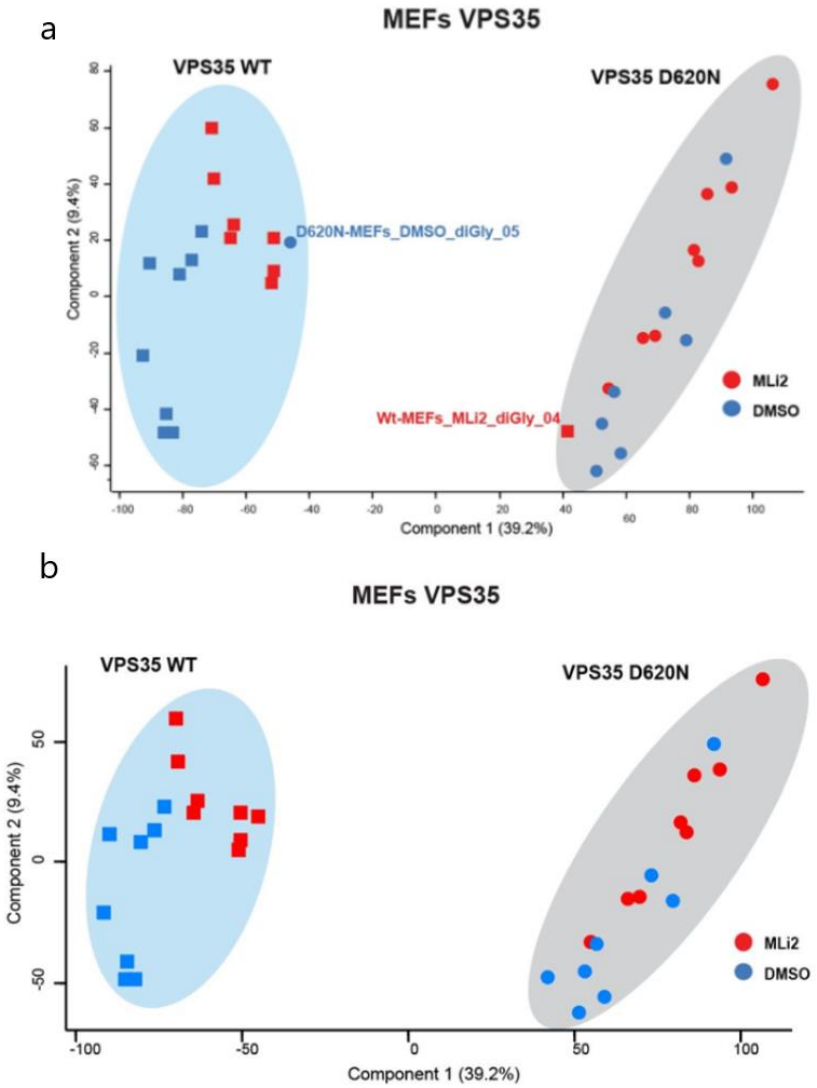

Figure 5.4 Principal Component Analysis of di-Gly enriched WT and VPS35 D620N ± MLi-2 samples (8 replicates per condition). (a) PCA shows that WT samples, displayed as rectangles, cluster altogether except for replicate #4 of MLi-2 treated group. All VPS35 [D620N] samples (as circles) cluster in a different area with the exception of replicate #5 of DMSO group. (b) PCA of di-Gly enriched WT and VPS35 D620N ± MLi-2 samples once outliers were removed from the analysis.

It was also noticed that within the VPS35 [D620N] group there was not a distinct clustering of DMSO samples apart from MLi-2 treated samples, unlike the WT. Therefore, the PCA was repeated just considering VPS35 [D620N] samples (**figure 5.5**). Data revealed that two DMSO replicates, #3 and #8, were clustering quite distantly from the others, while three MLi-2 replicates, #2, #5, and #6, were found to be grouped with the DMSO samples (**figure 5.5*a***). Therefore, it was chosen to eliminate the outliers while retaining only the ones that produce reliable results (**figure 5.5*b***).

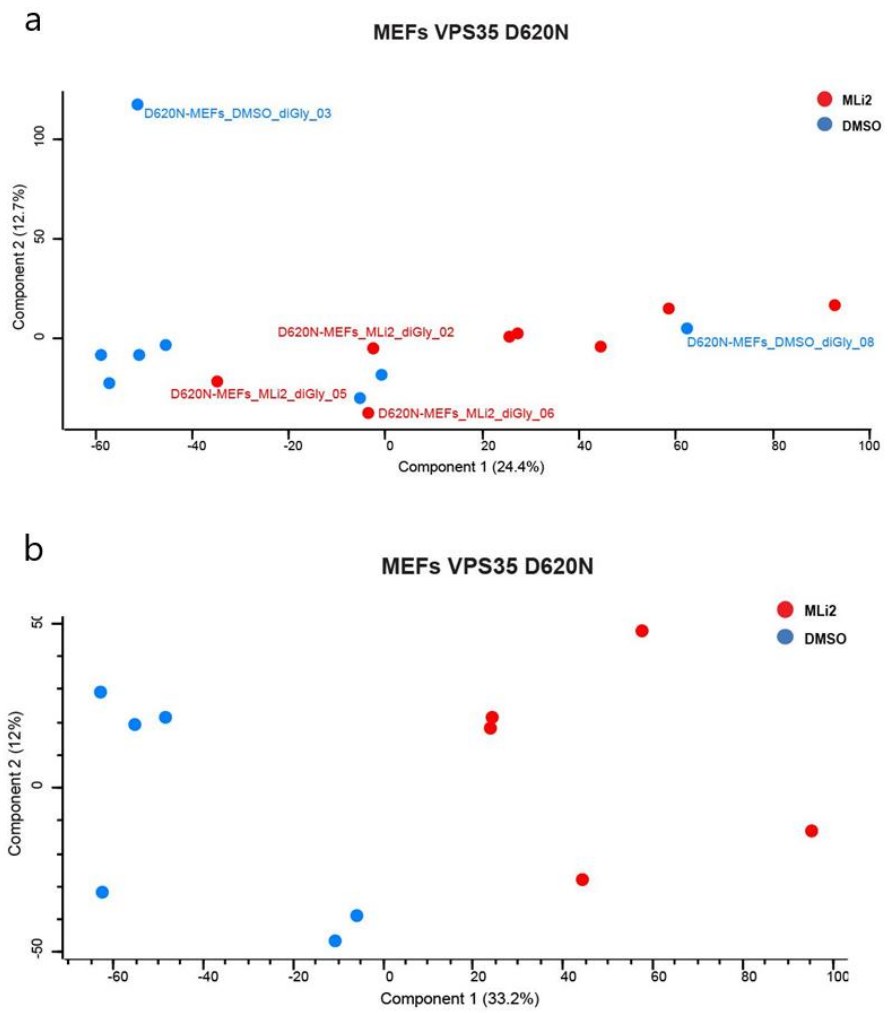

Figure 5.5 PCA of only di-Gly enriched VPS35 [D620N] ± MLi-2 samples (8 replicates per condition). (a) DMSO treated samples cluster relatively together on the left side of the graph apart from replicates #3 and #8. On the right side, cluster MLi-2 treated samples except for replicates #2, #5 and #6. (b) PCA of di-Gly enriched VPS35 [D620N] ± MLi-2 samples once all the outliers were excluded from the analysis.

Once analyzed through Perseus, data were visualized using Curtain software. Different protein expression between WT and VPS35 [D620N] not treated samples, was illustrated using a volcano plot (**figure 5.6*a***). Ubiquitylated proteins whose levels increase with the [D620N] mutation are specifically labelled. Some proteins are associated with the LRRK2 signalling pathway (in red), including SPAG9 and RILPL1, while other significantly regulated proteins such as TRIM47, GJB2, and SLC38A4 are annotated to highlight their potential relevance to the [D620N] variant. The second volcano plot still compares the [D620N] mutant to WT under DMSO treatment, focusing specifically on LRRK2 pathway-related proteins (**figure 5.6*b***). Several RAB family members (Rab7a, Rab10, Rab3b, and Rab8b) and RILPL1 are significantly enriched, suggesting increased ubiquitylation in the [D620N] variant compared to WT. These findings confirm that the [D620N] mutation enhances LRRK2 kinase activity, resulting in higher ubiquitylation of substrates.

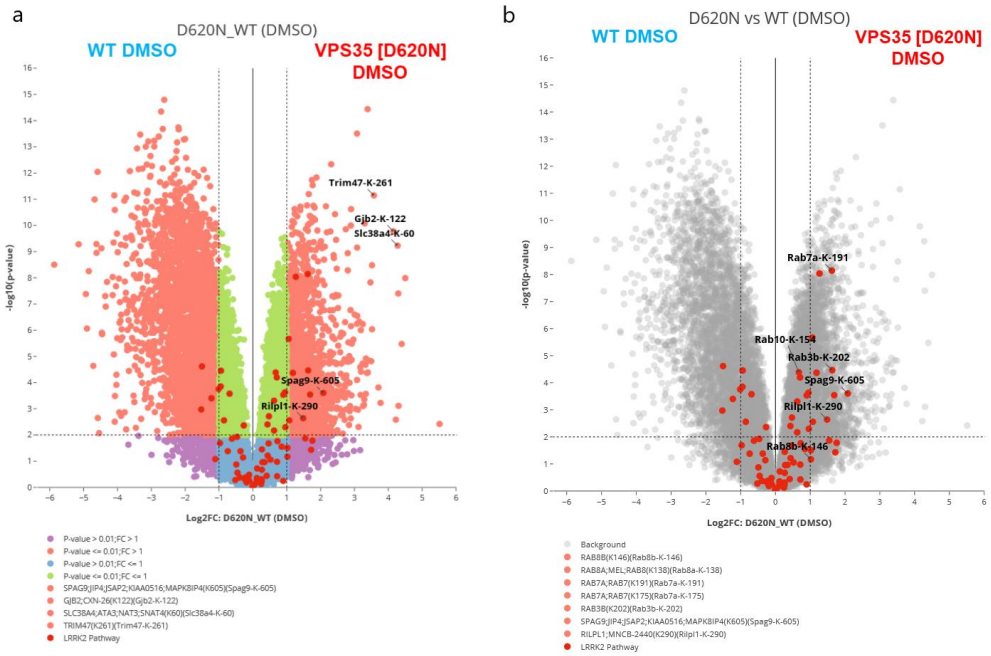

Figure 5.6 Volcano plots of di-Gly enriched WT and VPS35 [D620N] DMSO samples. (a) Significantly upregulated proteins ($p \leq 0.01$, fold change > 1) are shown in light red and

downregulated proteins in green (p≤ 0.01, fold change ≤ 1). Key proteins are highlighted. (b) Volcano plot highlighting LRRK2 pathway–related proteins (shown in dark red) compared to the overall background (grey). Several RAB family members and RILPL1-K290 show significant enrichment, indicating enhanced LRRK2-dependent phosphorylation in the D620N variant. Data can be visualized at this link: https://curtainptm.proteo.info/#/68674faf-b5a4-42f9-af86-8e5f19f2b930.

Next, a comparison was made between DMSO- and MLi-2-treated VPS35 [D620N] samples. Data revealed a reduced number of ubiquitylated proteins after MLi-2 treatment, which suggests that if LRRK2 is inhibited, these proteins may be recovered (**figure 5.7*a***). This trend is repeated when LRRK2 pathway-related proteins are looked at closely (**figure 5.7*b***).

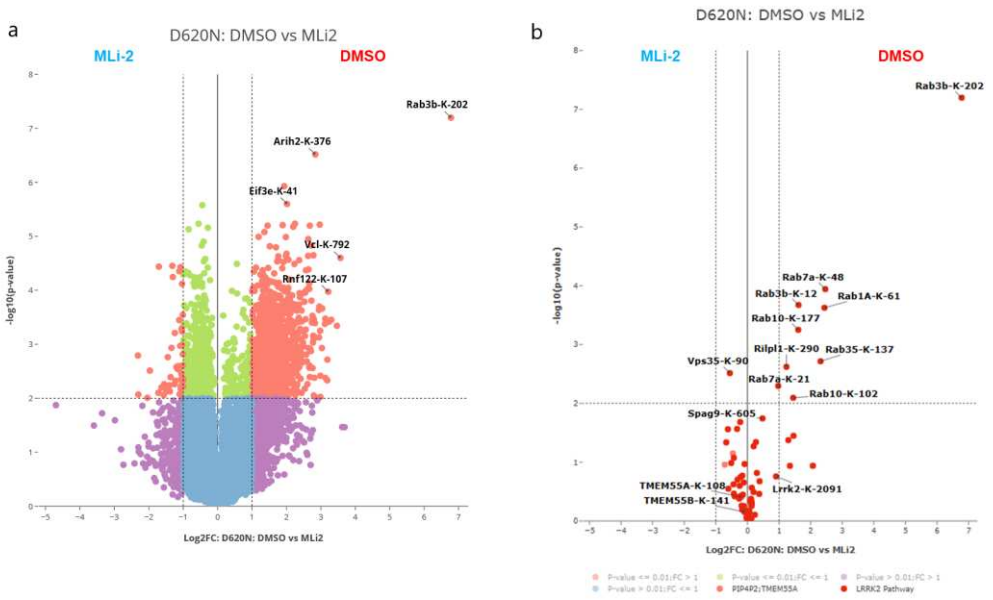

Figure 5.7 Volcan plots of di-Gly enriched VPS35 [D620N] comparing DMSO and MLi-2 treated samples profiles. (a) Significantly upregulated proteins (p ≤ 0.01, fold change > 1) are shown in light red and downregulated proteins in green (p≤ 0.01, fold change ≤ 1). The MLi-2 treatment results in a reduced number of ubiquitylated proteins, suggesting that inhibiting LRRK2 may allow for their recovery. (b) Volcano plot highlighting LRRK2 pathway–related proteins, shown in dark red. Data can be visualized at this link: https://curtainptm.proteo.info/#/68674faf-b5a4-42f9-af86-8e5f19f2b930.

Lastly, WT DMSO- and MLi-2-treated samples were compared. In this case, when treated with MLi-2 and LRRK2 activity is inhibited, there is no significant difference compared to untreated cells (**figure 5.8*a***). Although, when looking closely at LRRK2 pathway-related proteins, DMSO samples show a higher rate of ubiquitylation (**figure 5.8*b***).

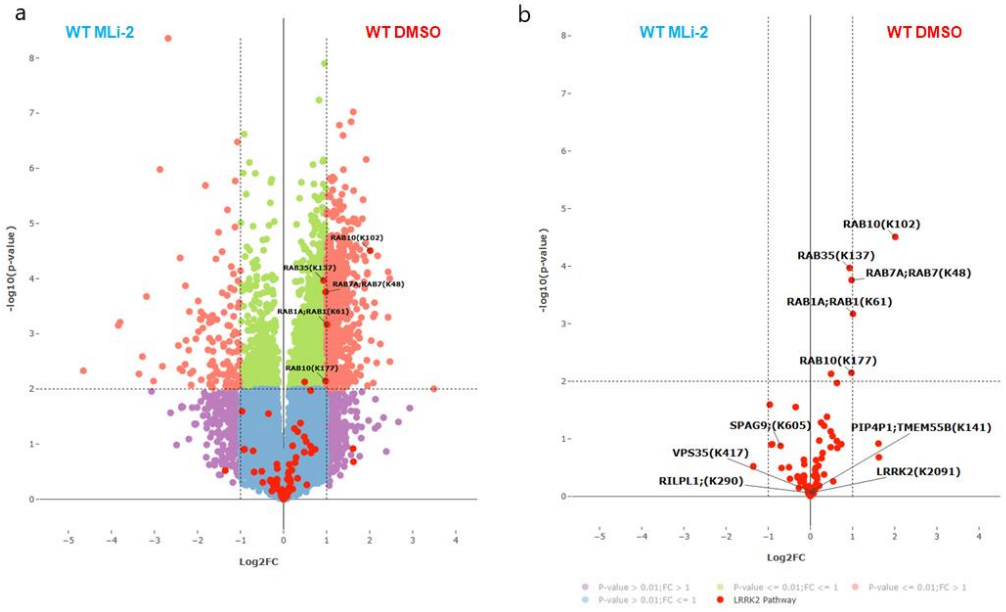

Figure 5.8 Volcano plots of di-Gly enriched WT ± MLi-2 samples. (a) Significantly upregulated proteins ($p \leq 0.01$, fold change > 1) are shown in light red and downregulated proteins in green ($p \leq 0.01$, fold change ≤ 1). Treating with MLi-2 results in a reduced number of ubiquitylated proteins. (b) Volcano plot highlighting LRRK2 pathway–related proteins, shown in dark red. Data can be visualized at this link: https://curtainptm.proteo.info/#/ca804f70-a428-4f66-ba4a-1e50fd893cde.

LRRK2 pathway components and Parkinson's Disease related genes ubiquitylation profiles were analyzed across experimental conditions. When WT and [D620N] samples were compared, LRRK2 components were more ubiquitylated in the mutant (**figure 5.9*a***). This means that, when LRRK2 is hyperactive in the presence of the mutation, more proteins involved in the LRRK2 pathway undergo ubiquitylation and may therefore be degraded by the proteasome. If LRRK2 activity is inhibited through MLi-2 treatment, ubiquitylation rates decrease suggesting a recovery of those proteins (**figure 5.9*b***). In particular, RILPL1 ubiquitylation levels returned to those of WT when treated with MLi-2 (**figure 5.10**).

On the other hand, PD-related genes were less ubiquitylated in the mutant background (**figure 5.11*a***). This could suggest that cell levels of those proteins are unbalanced and that proteasomal degradation is reduced.

Once again, when VPS35 [D620N] were treated with MLi-2 and LRRK2 activity was inhibited, fewer proteins underwent ubiquitylation and might have been rescued (**figure 5.11*b***).

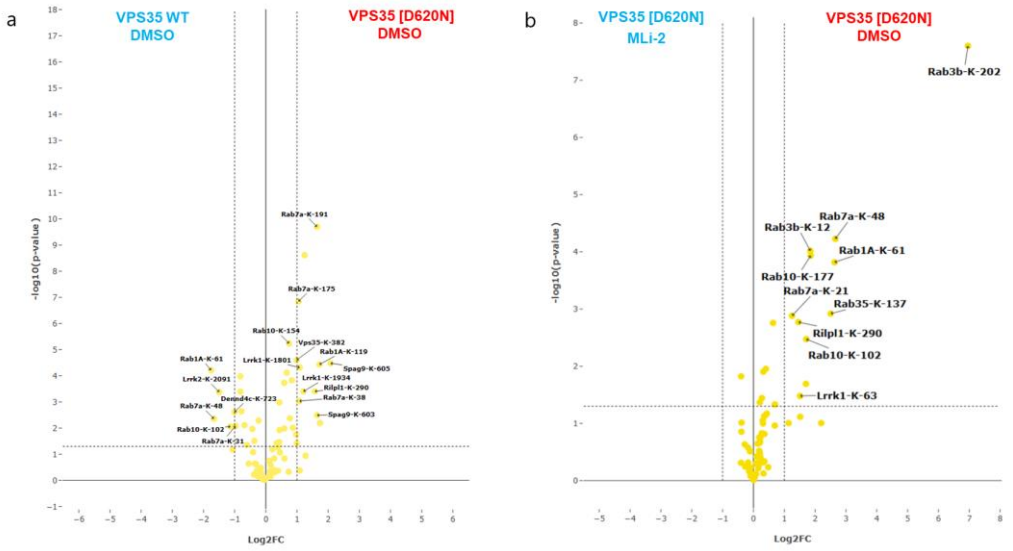

Figure 5.9 Comparison of LRRK2 pathway components. (a) Volcano plot of di-Gly enriched LRRK2-pathway related proteins in WT vs VPS35 [D620N] samples. (b) Volcano plot of di-Gly enriched VPS35 [D620N] ± MLi-2 samples highlighting LRRK2-pathway related proteins.

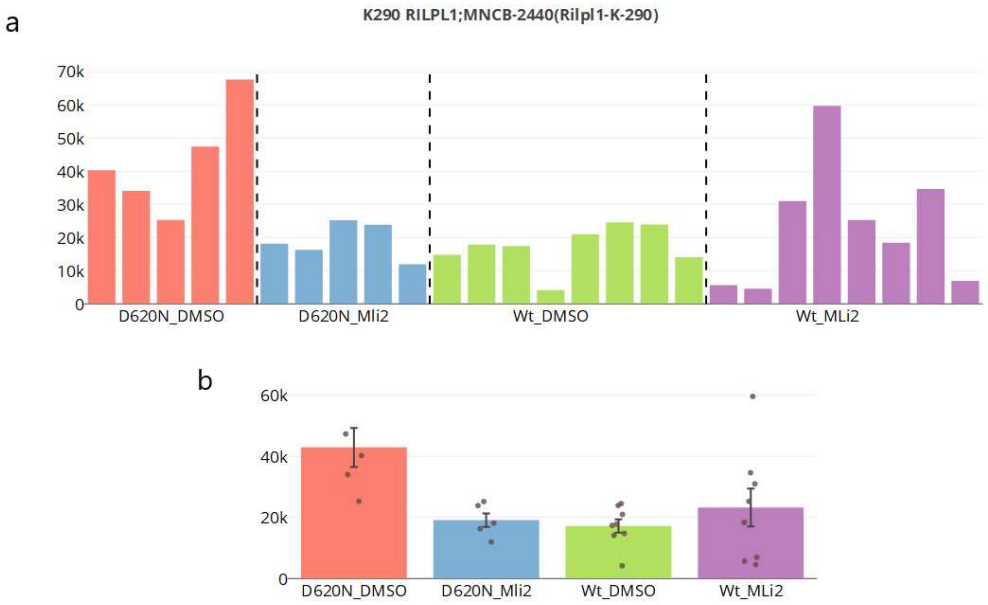

Figure 5.10 Bar chart of RILPL1 ubiquitylation levels at K-290 residue across all samples (a) and across experimental conditions (b).

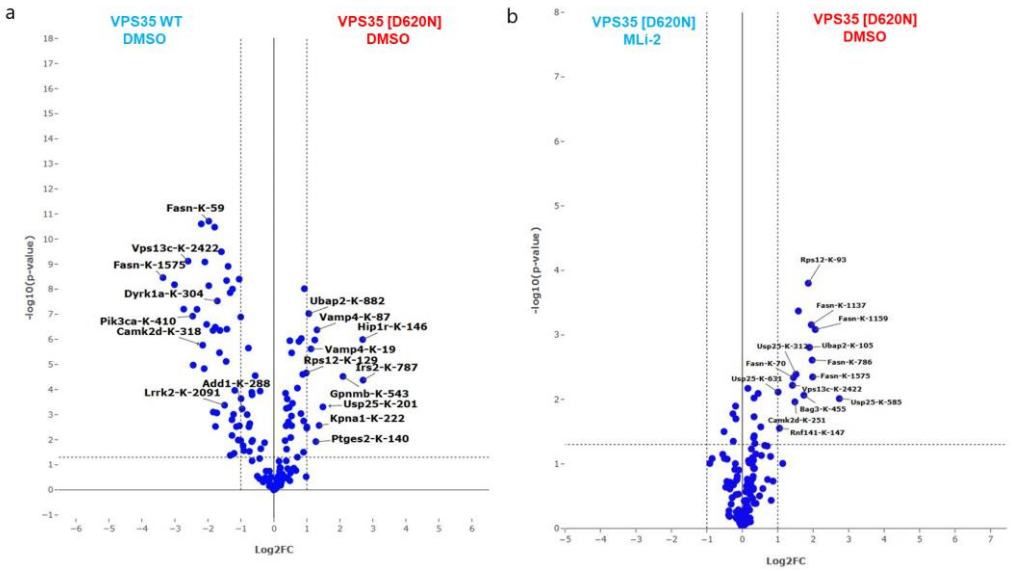

Figure 5.11 Comparison of Parkinson's Disease related genes. (a) Volcano plot of di-Gly enriched PD related proteins in WT vs VPS35 [D620N] samples. (b) Volcano plot of di-Gly enriched VPS35 [D620N] ± MLi-2 samples highlighting PD related proteins.

The binding of pRab10 to RILPL1 interferes with the formation of primary cilium in the somatosensory cortex and in the dorsal striatum, altering the Hedgehog signalling which is important to provide neuroprotective factors to DOPA neurons. [28] For this very reason, the ubiquitylation profiles of Hedgehog signalling-related genes were analyzed across experimental conditions (**figure 5.12**). Treatment of VPS35 [D620N] samples with MLi-2 once again decreased the ubiquitylation of proteins related to the Hedgehog signalling pathway, suggesting a recovery in their cellular levels (**figure 5.12*b***). This trend was also observed when analysing ubiquitylation levels of E ligases components (**figure 5.13**).

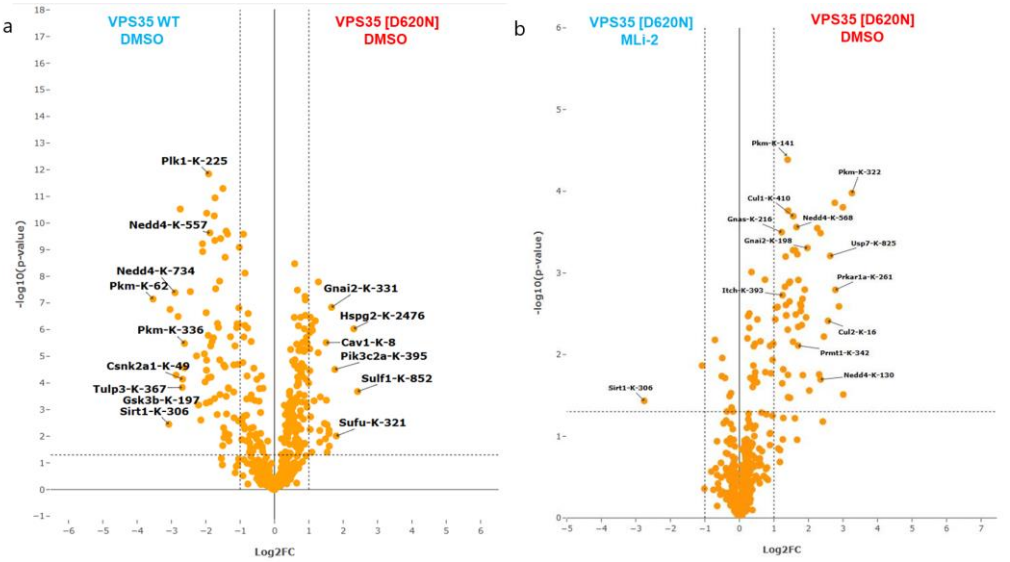

Figure 5.12 Comparison of Hedgehog signalling related genes. (a) Volcano plot of di-Gly enriched Hedgehog-pathway related proteins in WT vs VPS35 [D620N] samples. (b) Volcano plot of di-Gly enriched VPS35 [D620N] ± MLi-2 samples highlighting Hedgehog related proteins.

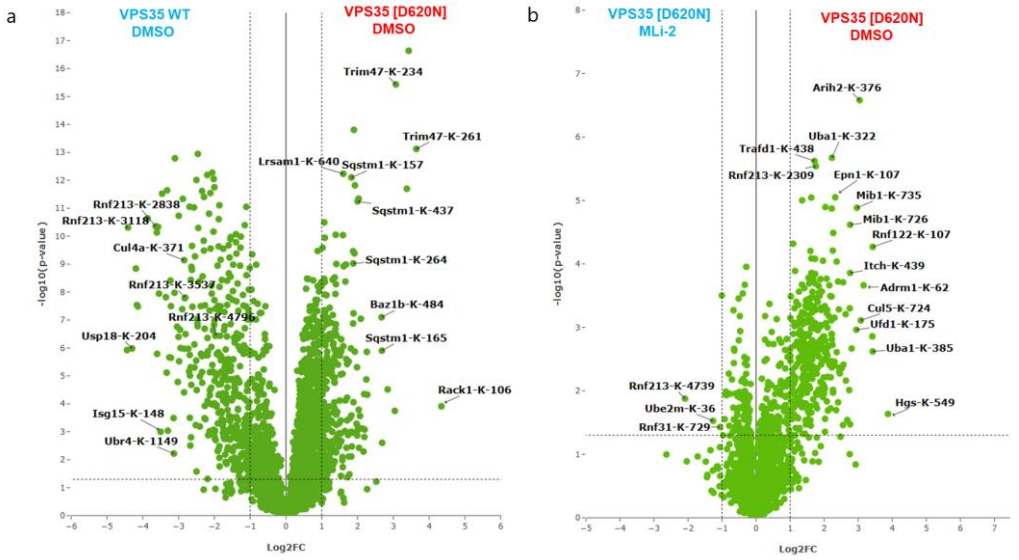

Figure 5.13 Comparison of UPS components (E1, E2 and E3 ligases). (a) Volcano plot of di-Gly enriched UPS proteins in WT vs VPS35 [D620N] samples. (b) Volcano plot of di-Gly enriched VPS35 [D620N] ± MLi-2 samples highlighting UPS related proteins.

Analysis of WT and VPS35 [D620N] total proteome

To better understand the full complexity of the system, the total proteome was also analyzed. Both WT and VPS35 [D620N] samples were digested with Trypsin/Lys-C and prepared for injection as described in the methods' section. For each replicate 2 µg of peptide were injected on an Orbitrap Astral spectrometer for DIA analysis. Data were searched through DIA-NN software and analyzed using Perseus. Approximately 10,150 protein groups were identified for WT and slightly less for the mutant (10,075 groups) across all experimental conditions. No significant change was observed between DMSO and MLi-2 treated samples within each group (**figure 5.14*a***). Reliability of sample preparation and data collection was proven through Pearson correlation analysis. The high correlation values ($r > 0.9$) observed between replicates demonstrate the reproducibility of the method and the consistency of the results obtained from the DIA-NN search within each condition (**figure 5.14*b***). Principal Component Analysis was performed on both WT and VPS35 [D620N] ± MLi-2 samples. The WT replicates grouped together, while the VPS35 [D620N] samples clustered separately. There were no significant

differences noted between DMSO- and MLi-2-treated within each respective group (**figure 5.14*c***).

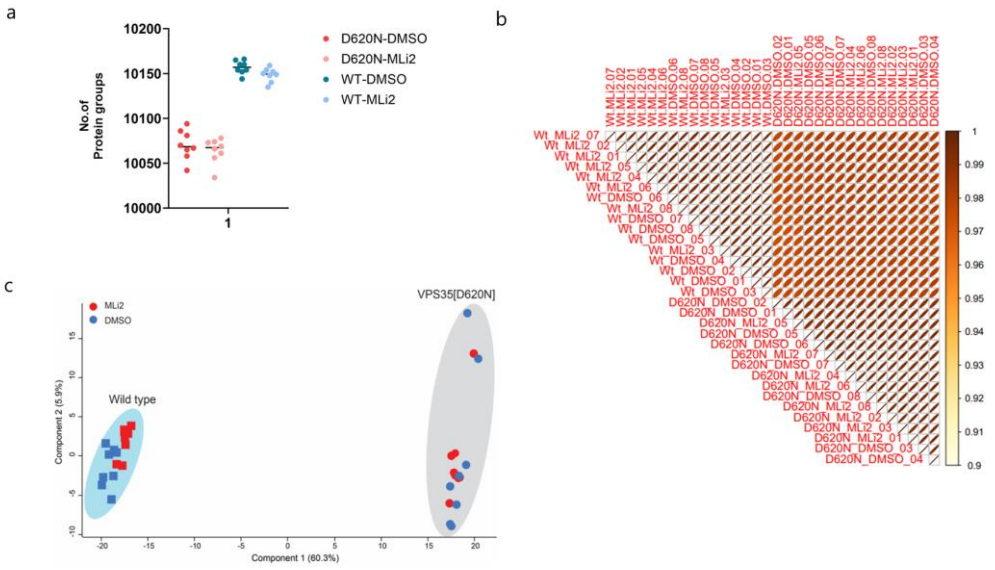

Figure 5.14 Results summary of total proteome analysis of WT and VPS35 [D620N] ± MLi-2 MEFs. (a) The total number of protein groups identified across experimental conditions (8 replicates per condition). Both WT DMSO (in green) and WT MLi-2 (in light blue) and VPS35 [D620N] DMSO (in red) and MLi-2 (in pink) samples were analyzed, ranging approximately 10,150 groups for WT and slightly less for the mutant (10,075 groups). No significant change was observed between DMSO and MLi-2 within each group. Each point represents an independent replicate. (b) Pairwise Pearson correlation heatmap highlighting the reproducibility among biological replicates within each condition. High correlation coefficients ($r > 0.9$) between replicates indicate a strong level of consistency in the DIA-NN search results. (c) Principal Component Analysis of WT and VPS35 D620N ± MLi-2 samples. On the left all WT replicates, both DMSO and MLi-2, cluster together while VPS35 [D620N] samples cluster together on the right side. No significant change was observed between DMSO and MLi-2 within each group.

Total proteome quantification was used to determine how inhibition of LRRK2 kinase activity affects steady-state protein abundance in WT and VPS35

[D620N] MEFs. Curtain software was used for the visualization of data. The volcano plots (**figure 5.15**) highlight clear, condition-specific changes in protein levels that mirror the alterations observed in the ubiquitinome.

Under basal conditions, VPS35 [D620N] cells displayed different abundance of several proteins associated with LRRK2 signalling compared to WT (**figure 5.15*a***). Proteins such as RILPL1/2, Rab10, Rab12, Rab29, and others were moderately reduced in [D620N] relative to WT. These decreases are consistent with the increased ubiquitylation observed in the ubiquitinome analysis, suggesting enhanced turnover or destabilization of these substrates when LRRK2 is hyperactive.

Following LRRK2 inhibition with MLi-2, many of the same LRRK2-related proteins showed a significant increase in abundance relative to [D620N]-DMSO (**figure 5.15*b***). The volcano plot reveals a right-shift for Rab12, Rab10, RILPL2, Rab7a, and several other LRRK2 substrates. This shift indicates that inhibiting LRRK2 restores protein levels that were reduced in the [D620N] mutation. Importantly, these increases reflect with the marked reduction in ubiquitylation of the same proteins, supporting the idea that LRRK2-dependent ubiquitylation promotes their degradation or reduces their stability.

In contrast, MLi-2 treatment in WT MEFs produced only limited changes in the abundance of LRRK2-associated proteins (**figure 5.15*c***). Most Rabs and RILPL proteins remained unchanged or only mildly affected. Instead, a separate set of stress-responsive (Nqo1, Gstm, Cyp)* or metabolic proteins (Ier5, Sgk1 and Enc1)** shifted in abundance. This demonstrates that the stabilizing effect of MLi-2 on LRRK2-substrate proteins is specific to the [D620N] hyperactive LRRK2 mutant rather than a general response to kinase inhibition.

---

* Nqo1: NAD(P)H quinone dehydrogenase 1
Gstm2 / Gstm1: Glutathione S-transferases
Cyp2j6, Cyp1b1: Cytochrome P450 enzymes

** Ier5: Immediate early response protein
Sgk1: Serum/glucocorticoid regulated kinase, induced by stress
Enc1: Ectodermal-neural cortex 1, redox-responsive protein

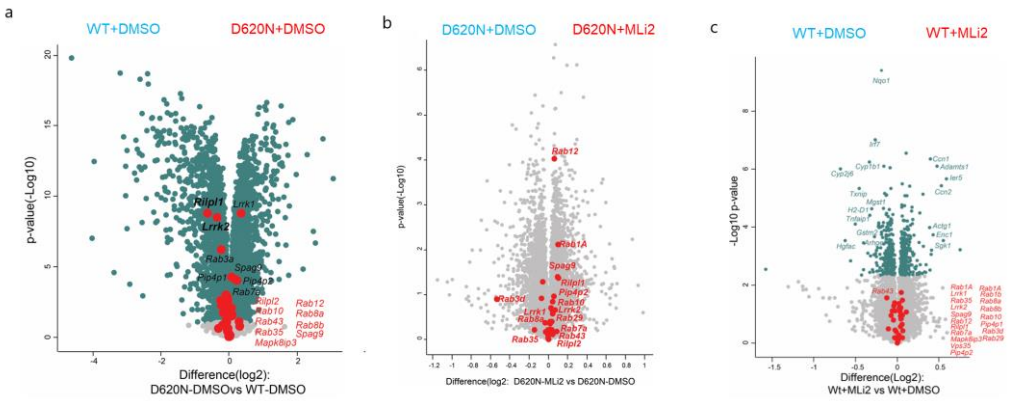

Figure 5.15 Results of MS total proteome analysis. LRRK2 related components are highlighted in red. (a) Volcano plot comparing WT vs VPS35 [D620N] total proteome profiles. (b) Volcano plot of VPS35 [D620N] total proteome comparing DMSO and MLi-2 treatments. (c) Volcano plot of WT total proteome comparing ± MLi-2.

6. Discussion and Conclusions

The aim of this work was to investigate the molecular mechanisms linking alterations in LRRK2 kinase activity to proteasomal degradation in Parkinson's disease.

Literature identified the VPS35 [D620N] mutation, which is associated with familial Parkinson's disease, as increasing LRRK2 kinase activity and reducing the content of lysosomal proteins.[30] However, the downstream consequences of this hyperactivation on the ubiquitin-proteasome system are still not completely understood.

The primary object of this thesis was to develop a global ubiquitinomics methodology based on di-Gly (K-ε-GG) peptide enrichment and apply it to determine how LRRK2 activity alters the ubiquitinome in mouse embryonic fibroblasts (MEFs) expressing either wild-type (WT) or [D620N]-mutant VPS35.

Three protocols, based on either 8M urea or 2% SDS or 1% SDC, were tested, and the resulting ubiquitinome profiles were compared (**figure 5.1**). The SDS-based methodology was chosen as the most suitable for the intended purpose, as it provides better solubilization of proteins and enables greater membrane protein coverage, along with a simple workflow. This method relies on the characteristic K-GG remnant of ubiquitylated peptides, which is recognized by monoclonal antibodies and identified by MS through a mass shift of 114.043 Da corresponding to the -GG adduct.

A comprehensive LRRK2 regulated global ubiquitinome data was generated. Ubiquitinome profiling of WT and VPS35 [D620N] MEFs revealed that a subset of proteins, associated with LRRK2-dependent endolysosomal trafficking such as RILPL1/2 and several Rabs, displayed increased

ubiquitylation in VPS35 [D620N] cells compared with WT controls (**figure 5.6**). This is consistent with the hyperactivation of LRRK2 kinase activity caused by the [D620N] mutation, which enhances phosphorylation of Rab substrates and can promote downstream ubiquitylation events.

Upon pharmacological inhibition of LRRK2 with MLi-2, the ubiquitylation of LRRK2-regulated substrates, along with Hedgehog- and PD-related proteins and UPS components, was markedly reduced (**figure 5.9** to **5.13**). This suggests that misregulated LRRK2 signalling is a contributing factor to their enhanced turnover or altered proteostasis in the [D620N] background.

To determine whether changes in ubiquitylation were linked to variations in protein levels, quantitative proteomics were conducted under the same experimental conditions. Strikingly, many of the proteins that experienced a reduction in ubiquitylation following MLi-2 treatment, showed a corresponding increase in their steady-state protein levels (**figure 5.15**).

Together, these data indicate that LRRK2 hyperactivation in VPS35 [D620N] MEFs promotes the ubiquitylation of specific Rab GTPases and interacting proteins, likely enhancing their degradation or otherwise destabilizing them. Pharmacological inhibition of LRRK2 reduces their ubiquitylation-associated turnover by stabilizing them. This supports a model in which LRRK2 kinase activity directly influences the ubiquitin-dependent turnover of multiple signalling components, and that pharmacological inhibition can rescue their steady-state levels.

Although promising results were observed, this research had its limitations. Most notably, the MLi-2 treatment was limited to just one hour, which was insufficient for the cell levels of the proteins whose expression was reduced in the mutant, to be restored back to those of the WT. Literature data showed that the minimum time required to completely restore RILPL1 levels was at least 24 hours (**figure 2.5*c***). For this reason, a possible future experiment could involve administering the pharmacological treatment for 24–48 hours.

Moreover, all analyses were performed using 1 mg of protein from cell lysates. To contain the costs of sample preparation, a possible future perspective would be to conduct a downscaling experiment, testing 500 μg and 100 μg of cell lysate as the initial sample size. Another possible approach would be to carry out a series of experiments to profile the ubiquitinome at the organelle level (e.g. Lyso-IPs) by adapting the enrichment method.

In addition to suggesting a methodology for studying LRRK2-regulated ubiquitinome in murine cells, this model could be used in other ubiquitinomics study within different tissues (e.g. nervous system cells).
Overall, these data open new important perspectives for understanding the downstream mechanisms of Parkinson's disease.

INDEX OF FIGURES

BIBLIOGRAPHY

[1] Y. Luo, L. Qiao, M. Li, X. Wen, W. Zhang, and X. Li, "Global, regional, national epidemiology and trends of Parkinson's disease from 1990 to 2021: findings from the Global Burden of Disease Study 2021," *Front Aging Neurosci*, vol. 16, 2024, doi: 10.3389/fnagi.2024.1498756.

[2] M. S. Khan, S. Nasiripour, and J. C. Bopassa, "Parkinson Disease Signaling Pathways, Molecular Mechanisms, and Potential Therapeutic Strategies: A Comprehensive Review," Jul. 01, 2025, *Multidisciplinary Digital Publishing Institute (MDPI)*. doi: 10.3390/ijms26136416.

[3] H. Braak, E. Ghebremedhin, U. Rüb, H. Bratzke, and K. Del Tredici, "Stages in the development of Parkinson's disease-related pathology," 2004. doi: 10.1007/s00441-004-0956-9.

[4] R. B. Postuma *et al.*, "Validation of the MDS clinical diagnostic criteria for Parkinson's disease," *Movement Disorders*, vol. 33, no. 10, 2018, doi: 10.1002/mds.27362.

[5] K. Vekrellis, M. Xilouri, E. Emmanouilidou, H. J. Rideout, and L. Stefanis, "Pathological roles of α-synuclein in neurological disorders," Nov. 2011. doi: 10.1016/S1474-4422(11)70213-7.

[6] X. Dong-Chen, C. Yong, X. Yang, S. T. Chen-Yu, and P. Li-Hua, "Signaling pathways in Parkinson's disease: molecular mechanisms and therapeutic interventions," Dec. 01, 2023, *Springer Nature*. doi: 10.1038/s41392-023-01353-3.

[7] D. J. Moore, A. B. West, V. L. Dawson, and T. M. Dawson, "Molecular pathophysiology of Parkinson's disease," 2005. doi: 10.1146/annurev.neuro.28.061604.135718.

[8] H. Deng, P. Wang, and J. Jankovic, “The genetics of Parkinson disease,” 2018. doi: 10.1016/j.arr.2017.12.007.

[9] D. G. Hernandez, X. Reed, and A. B. Singleton, “Genetics in Parkinson disease: Mendelian versus non-Mendelian inheritance,” 2016. doi: 10.1111/jnc.13593.

[10] J. Schapansky, J. D. Nardozzi, and M. J. Lavoie, “The complex relationships between microglia, alpha-synuclein, and LRRK2 in Parkinson’s disease,” 2015. doi: 10.1016/j.neuroscience.2014.09.049.

[11] M. Steger *et al.*, “Phosphoproteomics reveals that Parkinson’s disease kinase LRRK2 regulates a subset of Rab GTPases,” *Elife*, vol. 5, 2016, doi: 10.7554/elife.12813.

[12] M. Steger *et al.*, “Systematic proteomic analysis of LRRK2-mediated rab GTPase phosphorylation establishes a connection to ciliogenesis,” *Elife*, vol. 6, 2017, doi: 10.7554/eLife.31012.

[13] A. H. Hutagalung and P. J. Novick, “Role of Rab GTPases in membrane traffic and cell physiology,” 2011. doi: 10.1152/physrev.00059.2009.

[14] D. R. Alessi and S. R. Pfeffer, “Leucine-Rich Repeat Kinases,” vol. 66, p. 18, 2025, doi: 10.1146/annurev-biochem-030122.

[15] A. Myasnikov *et al.*, “Structural analysis of the full-length human LRRK2,” *Cell*, vol. 184, no. 13, 2021, doi: 10.1016/j.cell.2021.05.004.

[16] S. S. Taylor and A. P. Kornev, “Protein kinases: Evolution of dynamic regulatory proteins,” 2011. doi: 10.1016/j.tibs.2010.09.006.

[17] D. R. Alessi and E. Sammler, “LRRK2 kinase in Parkinson’s disease,” 2018, *American Association for the Advancement of Science*. doi: 10.1126/science.aar5683.

[18] C. Krüger *et al.*, “MDSGene update and expansion: Clinical and genetic spectrum of *LRRK2* variants in Parkinson’s disease,” Dec. 10, 2024. doi: 10.1101/2024.12.10.24318787.

[19] A. F. Kalogeropulou *et al.*, “Impact of 100 LRRK2 variants linked to Parkinson’s disease on kinase activity and microtubule binding,” *Biochemical Journal*, vol. 479, no. 17, 2022, doi: 10.1042/BCJ20220161.

[20] N. Dzamko *et al.*, “Inhibition of LRRK2 kinase activity leads to dephosphorylation of Ser 910/Ser935, disruption of 14-3-3 binding and altered cytoplasmic localization,” *Biochemical Journal*, vol. 430, no. 3, 2010, doi: 10.1042/BJ20100784.

[21] R. J. Nichols *et al.*, “14-3-3 Binding to LRRK2 is disrupted by multiple Parkinson’s disease-associated mutations and regulates cytoplasmic localization,” *Biochemical Journal*, vol. 430, no. 3, 2010, doi: 10.1042/BJ20100483.

[22] D. Jennings *et al.*, “Preclinical and clinical evaluation of the LRRK2 inhibitor DNL201 for Parkinson’s disease,” *Sci Transl Med*, vol. 14, no. 648, 2022, doi: 10.1126/scitranslmed.abj2658.

[23] Y. Liu and N. S. Gray, “Rational design of inhibitors that bind to inactive kinase conformations,” 2006. doi: 10.1038/nchembio799.

[24] E. T. Williams, X. Chen, and D. J. Moore, “VPS35, the retromer complex and Parkinson’s disease,” 2017, *IOS Press*. doi: 10.3233/JPD-161020.

[25] X. Chen *et al.*, “Parkinson’s disease-linked D620N VPS35 knockin mice manifest tau neuropathology and dopaminergic neurodegeneration,” *Proc Natl Acad Sci U S A*, vol. 116, no. 12, 2019, doi: 10.1073/pnas.1814909116.

[26] R. Mir *et al.*, “The Parkinson’s disease VPS35[D620N] mutation enhances LRRK2-mediated Rab protein phosphorylation in mouse and human,” *Biochemical Journal*, vol. 475, no. 11, 2018, doi: 10.1042/BCJ20180248.

[27] D. Waschbüsch, E. Purlyte, P. Pal, E. McGrath, D. R. Alessi, and A. R. Khan, “Structural Basis for Rab8a Recruitment of RILPL2 via LRRK2 Phosphorylation of Switch 2,” *Structure*, vol. 28, no. 4, 2020, doi: 10.1016/j.str.2020.01.005.

[28] S. S. Khan *et al.*, “Pathogenic lrrk2 control of primary cilia and hedgehog signaling in neurons and astrocytes of mouse brain,” *Elife*, vol. 10, 2021, doi: 10.7554/eLife.67900.

[29] R. Fasiczka, Y. Naaldijk, B. Brahmia, and S. Hilfiker, “Insights into the cellular consequences of LRRK2-mediated Rab protein phosphorylation,” 2023. doi: 10.1042/BST20201145.

[30] P. Pal *et al.*, “Parkinson’s VPS35[D620N] mutation induces LRRK2-mediated lysosomal association of RILPL1 and TMEM55B,” 2023, doi: 10.5281/zenodo.

[31] K. N. Swatek and D. Komander, “Ubiquitin modifications,” 2016. doi: 10.1038/cr.2016.39.

[32] P. Roos-Mattjus and L. Sistonen, “The ubiquitin-proteasome pathway,” 2004. doi: 10.1080/07853890310016324.

[33] C. Naujokat and S. Hoffmann, “Role and function of the 26S proteasome in proliferation and apoptosis,” 2002. doi: 10.1097/01.LAB.0000022226.23741.37.

[34] S. S. Wing, “Deubiquitinating enzymes - The importance of driving in reverse along the ubiquitin-proteasome pathway,” 2003. doi: 10.1016/S1357-2725(02)00392-8.

[35] E. Oh, D. Akopian, and M. Rape, “Principles of Ubiquitin- Dependent Signaling,” 2018. doi: 10.1146/annurev-cellbio-100617-062802.

[36] R. Aebersold and M. Mann, “Mass-spectrometric exploration of proteome structure and function,” 2016. doi: 10.1038/nature19949.

[37] N. D. Udeshi, P. Mertins, T. Svinkina, and S. A. Carr, “Large-scale identification of ubiquitination sites by mass spectrometry,” *Nat Protoc*, vol. 8, no. 10, 2013, doi: 10.1038/nprot.2013.120.

[38] M. Steger, Ö. Karayel, and V. Demichev, “Ubiquitinomics: History, methods, and applications in basic research and drug discovery,” 2022. doi: 10.1002/pmic.202200074.

[39] J. Peng *et al.*, “A proteomics approach to understanding protein ubiquitination,” *Nat Biotechnol*, vol. 21, no. 8, 2003, doi: 10.1038/nbt849.

[40] Y. Shi, D. W. Chan, S. Y. Jung, A. Malovannaya, Y. Wang, and J. Qin, “A data set of human endogenous protein ubiquitination sites,” *Molecular and Cellular Proteomics*, vol. 10, no. 5, 2011, doi: 10.1074/mcp.M110.002089.

[41] D. Meierhofer, X. Wang, L. Huang, and P. Kaiser, “Quantitative analysis of global ubiquitination in HeLa cells by mass spectrometry,” *J Proteome Res*, vol. 7, no. 10, 2008, doi: 10.1021/pr800468j.

[42] J. M. R. Danielsen *et al.*, “Mass spectrometric analysis of lysine ubiquitylation reveals promiscuity at site level,” *Molecular and Cellular Proteomics*, vol. 10, no. 3, 2011, doi: 10.1074/mcp.M110.003590.

[43] G. Xu, J. S. Paige, and S. R. Jaffrey, “Global analysis of lysine ubiquitination by ubiquitin remnant immunoaffinity profiling,” *Nat Biotechnol*, vol. 28, no. 8, 2010, doi: 10.1038/nbt.1654.

[44] S. A. Wagner *et al.*, “Proteomic analyses reveal divergent ubiquitylation site patterns in murine tissues,” *Molecular and Cellular Proteomics*, vol. 11, no. 12, 2012, doi: 10.1074/mcp.M112.017905.

[45] N. D. Udeshi *et al.*, “Refined preparation and use of anti-diglycine remnant (k-ε-gg) antibody enables routine quantification of 10,000s of ubiquitination sites in single proteomics experiments,” *Molecular and Cellular Proteomics*, vol. 12, no. 3, 2013, doi: 10.1074/mcp.O112.027094.

[46] G. C. McAlister *et al.*, “MultiNotch MS3 enables accurate, sensitive, and multiplexed detection of differential expression across cancer cell line proteomes,” *Anal Chem*, vol. 86, no. 14, 2014, doi: 10.1021/ac502040v.

[47] G. C. McAlister *et al.*, “Increasing the multiplexing capacity of TMTs using reporter ion isotopologues with isobaric masses,” *Anal Chem*, vol. 84, no. 17, 2012, doi: 10.1021/ac301572t.

[48] W. Kim *et al.*, “Systematic and quantitative assessment of the ubiquitin-modified proteome,” *Mol Cell*, vol. 44, no. 2, 2011, doi: 10.1016/j.molcel.2011.08.025.

[49] V. Akimov *et al.*, “Ubisite approach for comprehensive mapping of lysine and n-terminal ubiquitination sites,” *Nat Struct Mol Biol*, vol. 25, no. 7, 2018, doi: 10.1038/s41594-018-0084-y.

[50] F. M. Hansen *et al.*, “Data-independent acquisition method for ubiquitinome analysis reveals regulation of circadian biology,” *Nat Commun*, vol. 12, no. 1, Dec. 2021, doi: 10.1038/s41467-020-20509-1.

[51] P. Sinitcyn *et al.*, “MaxDIA enables library-based and library-free data-independent acquisition proteomics,” *Nat Biotechnol*, vol. 39, no. 12, 2021, doi: 10.1038/s41587-021-00968-7.

[52] V. Demichev, C. B. Messner, S. I. Vernardis, K. S. Lilley, and M. Ralser, “DIA-NN: neural networks and interference correction enable deep proteome coverage in high throughput,” *Nat Methods*, vol. 17, no. 1, 2020, doi: 10.1038/s41592-019-0638-x.

[53] S. Tyanova *et al.*, “The Perseus computational platform for comprehensive analysis of (prote)omics data,” 2016. doi: 10.1038/nmeth.3901.

[54] T. K. Phung *et al.*, “CURTAIN—A unique web-based tool for exploration and sharing of MS-based proteomics data,” *Proc Natl Acad Sci U S A*, vol. 121, no. 7, 2024, doi: 10.1073/pnas.2312676121.